Chemical Engineering Journal 505 (2025) 159467

Contents lists available at ScienceDirect

Chemical Engineering Journal

journal homepage: www.elsevier.com/locate/cej

Tunable and functional ionic liquids embedded hyper-crosslinked polymers as robust H_2O-tolerant adsorbents for highly efficient gaseous toluene capture

Xiongfei Nie [a,1], Xinjie Qiu [a,1], Ruina Zhang [a], Quanli Ke [a], Huayan Liu [a], Xiangping Zhang [b], Hanfeng Lu [a,*], Guokai Cui [a,*], Suojiang Zhang [b]

[a] Innovation Team of Air Pollution Control, Institute of Catalytic Reaction Engineering, Zhejiang Key Laboratory of Surface and Interface Science and Engineering for Catalysts, State Key Laboratory Breeding Base of Green Chemistry Synthesis Technology, College of Chemical Engineering, Zhejiang University of Technology, Hangzhou 310014, China

[b] Beijing Key Laboratory of Ionic Liquids Clean Process, CAS Key Laboratory of Green Process and Engineering, State Key Laboratory of Multiphase Complex Systems, Institute of Process Engineering, Chinese Academy of Sciences, Beijing 100190, China

ARTICLE INFO

Keywords:
Ionic liquid
Toluene
Volatile organic compound
Dual-site Langmuir-Freundlich model
Porous organic polymer

ABSTRACT

A series of tunable and functional ionic liquids embedded hyper-crosslinked polymers (ILHCPs) containing different structures of anion-functional ionic liquids (ILs) with 1,4-dichloroxylene (DCX) as the crosslinker were designed and prepared for highly efficient gaseous toluene adsorption under humidity. These ILHCPs could achieve high surface area (600 ~ 900 $m^2\ g^{-1}$), high micropore volume (0.1 ~ 0.3 $cm^3\ g^{-1}$), small average pore size (4 ~ 5 nm), large water contact angle (up to 110°), and high thermal stability (>350 °C) through tuning the anion structures and the initial IL:DCX molar ratio. Gaseous toluene adsorption isotherms were well described by a dual-site Langmuir-Freundlich (DSLF) model, and the isosteric heats were calculated. The selectivity of gaseous toluene for 80 % humidity was calculated to be 0.26, two times of typical metal–organic frameworks MIL-101 (0.12), and it increase with the decrease of humidity. Compared with DCX-based self-condensed HCP, toluene adsorption capacity of ILHCPs remained steadily (270 mg g^{-1}) even under 80 % humidity. The results of experiments and quantum chemical calculations indicated that anion is the main reason for efficient toluene adsorption under high humidity. Moreover, after the pre-treatments (acid treatment, alkali treatment, adsorption 1 % H_2O, and adsorption 5 % H_2O), the robust ILHCPs showed a good chemical stability and a stable adsorption capacity. Adsorption-desorption reversible cycles without capacity decrease indicated the good repeatability of ILHCPs. To our best knowledge, this is the first example of tuning functional ILHCPs for efficient H_2O-tolerant gaseous toluene adsorption. The method may open a door to achieve efficient and robust IL-based materials.

1. Introduction

Due to the widely used organic solvents in various industrial processes, the concentrations of volatile organic compounds (VOCs) in the atmosphere are increasing, and these VOCs have triggered a series of problems that threatens environment and human health, especially in some developing countries. Among VOCs, aromatic VOCs, such as benzene, toluene, and xylenes (BTX) have received more attention because of their known hazardous [1]. For example, benzene could cause DNA damage while toluene and xylenes associated with hearing disorders and neurological problems [2]. Moreover, many research work studied the uptake of VOCs by porous materials under dry conditions [3–5], but water vapor is omnipresent within the environment [6], and is present in indoor spaces at concentrations several orders of magnitude greater than the concentrations of VOCs. Thus, humidity is a key influential factor that affect the physical or chemical processes related to VOC emissions [7,8]. For most VOC adsorption materials, water vapor will reduce their VOCs adsorption capacity in a humid atmosphere [9,10]. Thus, developing efficient sorbents for efficient aromatic VOCs sorption from humid conditions are highly desired.

Ionic liquids (ILs) are known as a kind of sustainable solvents with tunable structures and unique properties, including high thermal and

* Corresponding authors.
E-mail addresses: luhf@zjut.edu.cn (H. Lu), chemcgk@163.com (G. Cui).
[1] These authors contributed equally to this work.

https://doi.org/10.1016/j.cej.2025.159467
Received 28 October 2024; Received in revised form 24 December 2024; Accepted 9 January 2025
Available online 10 January 2025

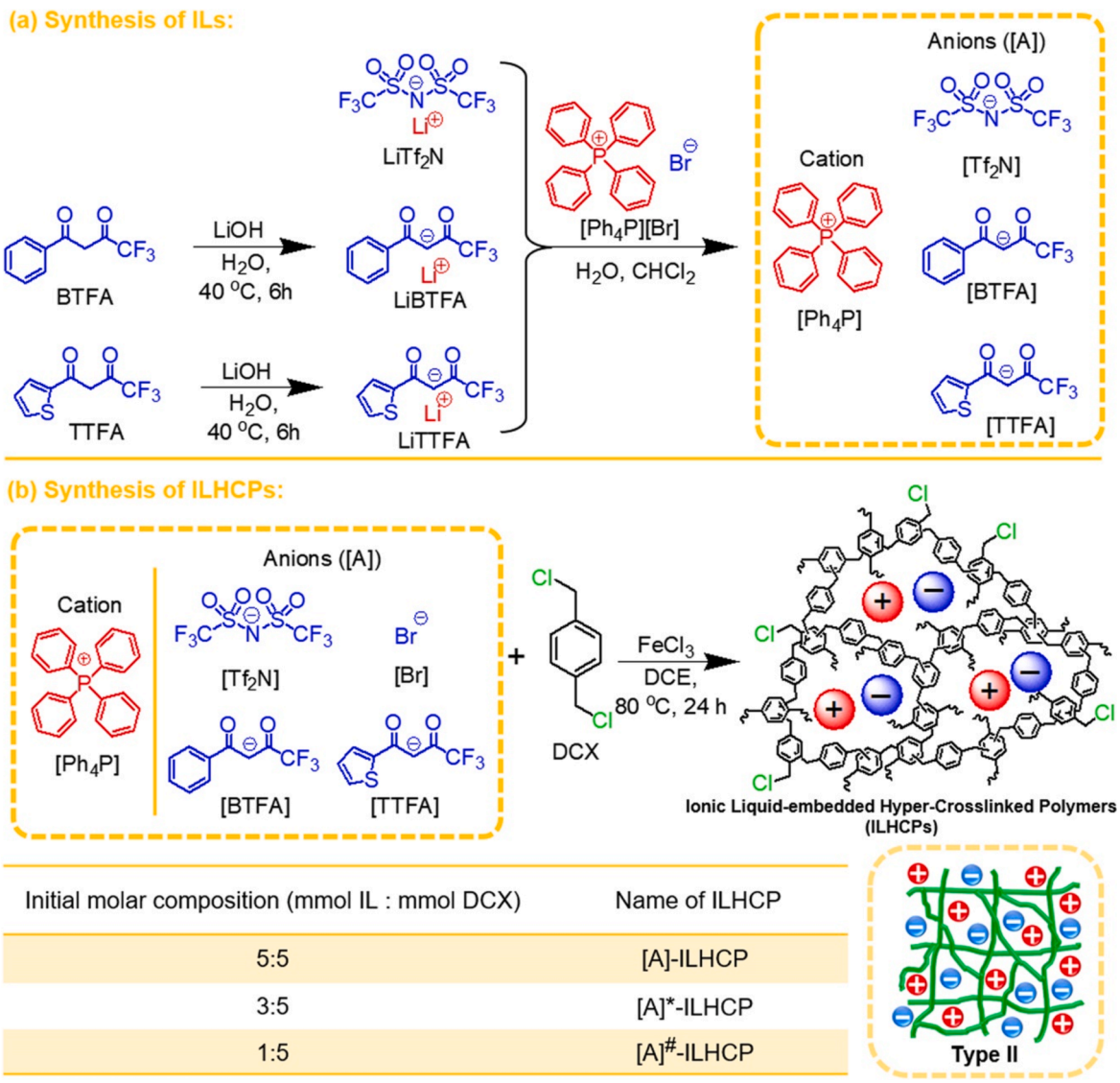

Initial molar composition (mmol IL : mmol DCX)	Name of ILHCP
5:5	[A]-ILHCP
3:5	[A]*-ILHCP
1:5	[A]#-ILHCP

Fig. 1. The synthesis and structures of ILHCPs.

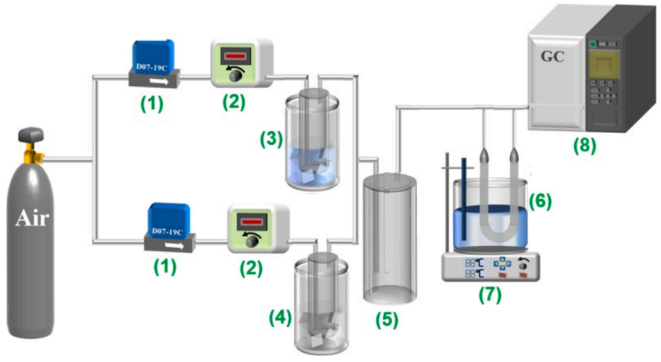

Fig. 2. Schematic diagram of the breakthrough experiments for gaseous toluene adsorption. (1) Mass flow meter, (2) flow controller, (3) humidifier, (4) gaseous toluene generator, (5) mixing tank, (6) U-tube, (7) temperature controller, (8) GC with FID.

chemical stability, low vapor pressure, and a strong ability to solubilize both inorganic and organic substances by choosing appropriate cations and anions. Theoretically, there are approximately 10^{18} room temperature ionic liquids available, which encompass both binary and ternary combinations [11]. Thus, ILs have been used as absorbents in capture and separation of gases, such as SO_2 [12–15], CO_2 [16–19], NO_x [20–23], NH_3 [24,25], CO [26–28], H_2S [29,30], and VOCs [31,32], as acetone [33], alcohols [34], chloroalkanes [35–37], chlorobenzene [38], benzene toluene and xylene (BTX) [39,40], *etc*. As a representative aromatic VOC, toluene vapor could be absorbed in tunable ILs. On one hand, kinds of ILs have been developed with such anions as tetrafluoroborate ($[BF_4]$) [41], hexafluorophosphate ($[PF_6]$) [42], bis(trifluoromethylsulfonyl)amide $[Tf_2N]$ [43], halides [44], carboxylates [45], sulfonates [46], sulfates [47], *etc*. Among these anions, $[Tf_2N]$ was found to be more efficient for toluene vapor absorption, compared with other anions [48,49] On the other hand, different cations also affect the sorption efficiency. For example, Dai *et al.* [50] reported that imidazolium-based ILs introduced into π-electron donors could achieve efficient toluene capture. Wang *et al.* [51] examined the impact of the type and length of the alkyl chain on the solubility of cations and anions in toluene. Although a report has shown that viscosity would decrease with increasing mole fraction of toluene in ILs [52], the viscosity of ILs themselves limits their industrial applications on VOCs sorption [53]. Thus, the development of alternative sorbents is necessary for toluene vapor capture. Recently, benzene ring-containing porous orgnic

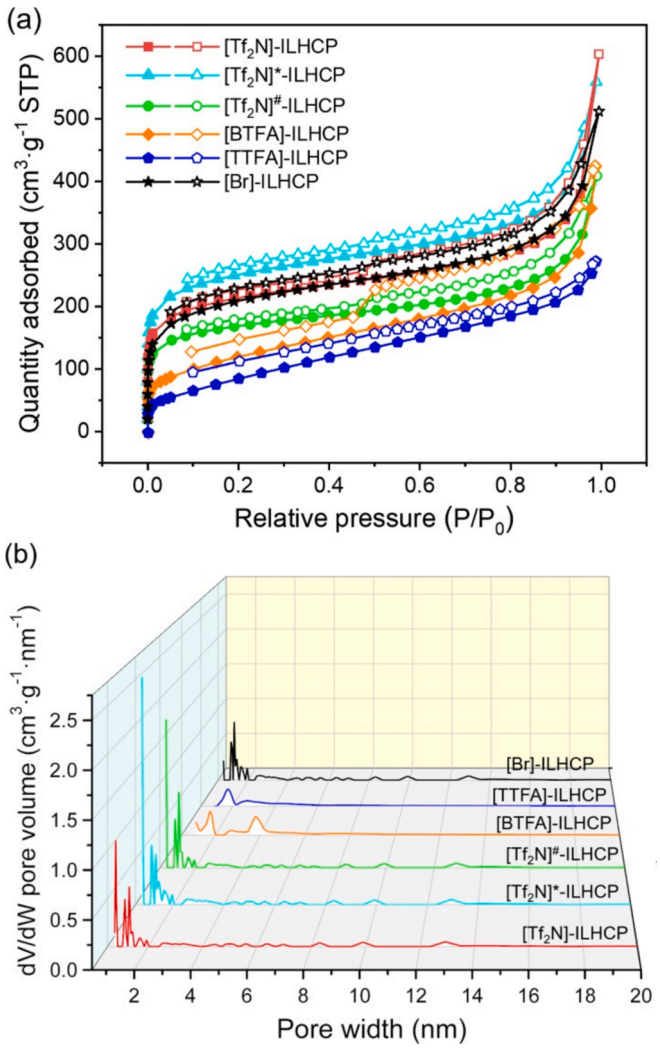

Fig. 3. N_2 adsorption–desorption isotherms at 77 K (a) and the pore distributions (b) of these ILHCPs.

Table 1
Initial molar composition (IL:DCX, in mmol:mmol), surface area (S_{BET}, in m^2 g^{-1}), total pore volume (V_{tot}, in cm^3 g^{-1}), micropore volume (V_{mic}, in cm^3 g^{-1}), average pore size (D, in nm), and water contact angle (θ, in °) of ILHCPs in this work.

HCP	IL:DCX	S_{BET}	V_{tot}	V_{mic}	D	θ
[Tf_2N]-ILHCP	5:5	772.5	0.93	0.17	4.8	110.5
[Tf_2N]*-ILHCP	3:5	909.9	0.86	0.32	3.8	80.5
[Tf_2N]$^{\#}$-ILHCP	1:5	612.9	0.63	0.20	4.1	42.2
[BTFA]-ILHCP	5:5	429.1	0.66	0.037	8.2	104.3
[TTFA]-ILHCP	5:5	318.8	0.42	0.007	9.8	110.7
[Br]-ILHCP	5:5	735.2	0.59	0.13	4.3	25.1

materials (POMs) have been applied for aromatic VOCs adsorption with tunable topology and pore size. These typical POMs include metal–organic frameworks (MOFs) [54,55], covalent organic frameworks (COFs) [56,57], covalent triazine frameworks (CTFs) [58], *etc*. Although these adsorbents seem to be promising, the expensive ligands as well as tedious preparation processes with low yields make them difficult to apply in industry. Recently, hyper-crosslinked polymers (HCPs) are developed as a kind of POMs which can be synthesized using inexpensive reagents, straightforward methods, and possess a highly crosslinked porous structure through the Friedel-Crafts alkylation process [59]. HCPs have found applications in separation and catalysts as sorbents and catalysts [60–64]. Based on the tailorability of ILs and porosity of HCPs, ILHCPs composites have been developed greatly during recent years [65]. However, none of ILHCPs has been developed for toluene adsorption, especially under humidity conditions. Thus, tuning the structure ILHCPs for efficient and selective gaseous toluene adsorption is highly desired [66].

Herein, a series of ILHCPs containing different structures of hydrophobic ILs with 1,4-dichloroxylene (DCX) as the crosslinker were designed and prepared *via* anion-exchange and Friedel-Crafts reaction for efficient gaseous toluene adsorption under humidity (Fig. 1). Hydrophobicity property as well as surface area, micropore volume, and average pore size of these ILHCPs were determined. Gaseous toluene adsorption isotherms on these ILHCPs were tested under 298, 308, and 318 K. A dual-site Langmuir-Freundlich (DSLF) model was used for well describing gaseous toluene adsorption, and the isosteric heats were calculated. Based on DSLF, equilibrium constant, Gibbs free energy change, enthalpy change, and entropy change of each adsorption site were calculated. Furthermore, toluene adsorption under different humidity conditions were also tested and exhibited steady adsorption capacity even under 80 % humidity. Quantum chemical calculations indicated the key role of the structures of anions in tunable adsorption performances. Moreover, different pre-treatment methods (acid treatment, alkali treatment, adsorption 1 % H_2O, and adsorption 5 % H_2O) were used to test and exhibiting the high chemical stability of ILHCPs. Desorption and adsorption–desorption cycles were measured and verify the reversibility of ILHCPs. Based on the information we know so far, this is the first example of tuning functional ILHCPs for efficient H_2O-tolerant gaseous toluene adsorption, which may open a door to achieving high adsorption efficiency of other VOCs by IL-based POPs.

2. Experimental methods

2.1. Materials

Tetraphenylphosphonium bromide ([Ph_4P][Br], 98 %, CAS No. 2751-90-8) was obtained from Shanghai Aladdin Biocherrical Technology Co., Ltd. Lithium bis(triluoromethanesultony)imide ($LiTf_2N$, 99.5 %, CAS No. 90076-65-6). Benzoyltrifluoroacetone (BTFA, 97 %, CAS No. 326-06-7) was obtained from Bide Pharmatech Ltd. while thenoyltrifluoroacetone (TTFA, 98 %, CAS No. 326-91-0) were procured from Meryer (Shanghai) Chemical Technology Co., Ltd. 1,4-Bis(chloromethyl)benzene (DCX, 98 %, CAS No. 623-25-6) and toluene (99.8 %, CAS No. 108-88-3) were obtained from Shanghai Macklin Biochemical Co., Ltd. 1,2-bichloroethane (DCE, 99 %, CAS No. 107-06-2) and ethanol (EtOH, 99.5 %, CAS No. 64–17-5) were approached from Shanghai Titan Scientific Co., Ltd. N_2 (99.99 %) were supplied from Hangzhou Jingong Gas Co., Ltd. Active carbon (AC-50) was supplied by Tangshan Tianhe activated carbon Co., Ltd.

2.2. Synthesis of ILs

Three kinds of anion-functional ILs were synthesized, including tetraphenylphosphonium bis(trifluoromethanesulfonyl)imide ([Ph_4P][Tf_2N]), tetraphenylphosphonium benzoyltrifluoroacetone ([Ph_4P][BTFA]), tetraphenylphosphonium thenoyltrifluoroacetone ([Ph_4P][TTFA]). All these ILs were all prepared by a same one-step anion-exchange method (Fig. 1). For example, [Ph_4P][Br] and $LiTf_2N$ at 1:1 M ratio were dissolve in water separately and organic phase was immediately obtained after mixing and stirring. DCE was used to dissolve organics. After separating the organic phase using a separatory funnel and washing with deionized water for 3 times to remove LiBr, the crude [Ph_4P][Tf_2N] in DCE was prepared. Then, neat [Ph_4P][Tf_2N] was obtained after removing the DCE and trance of water by rotary evaporation and freeze drying.

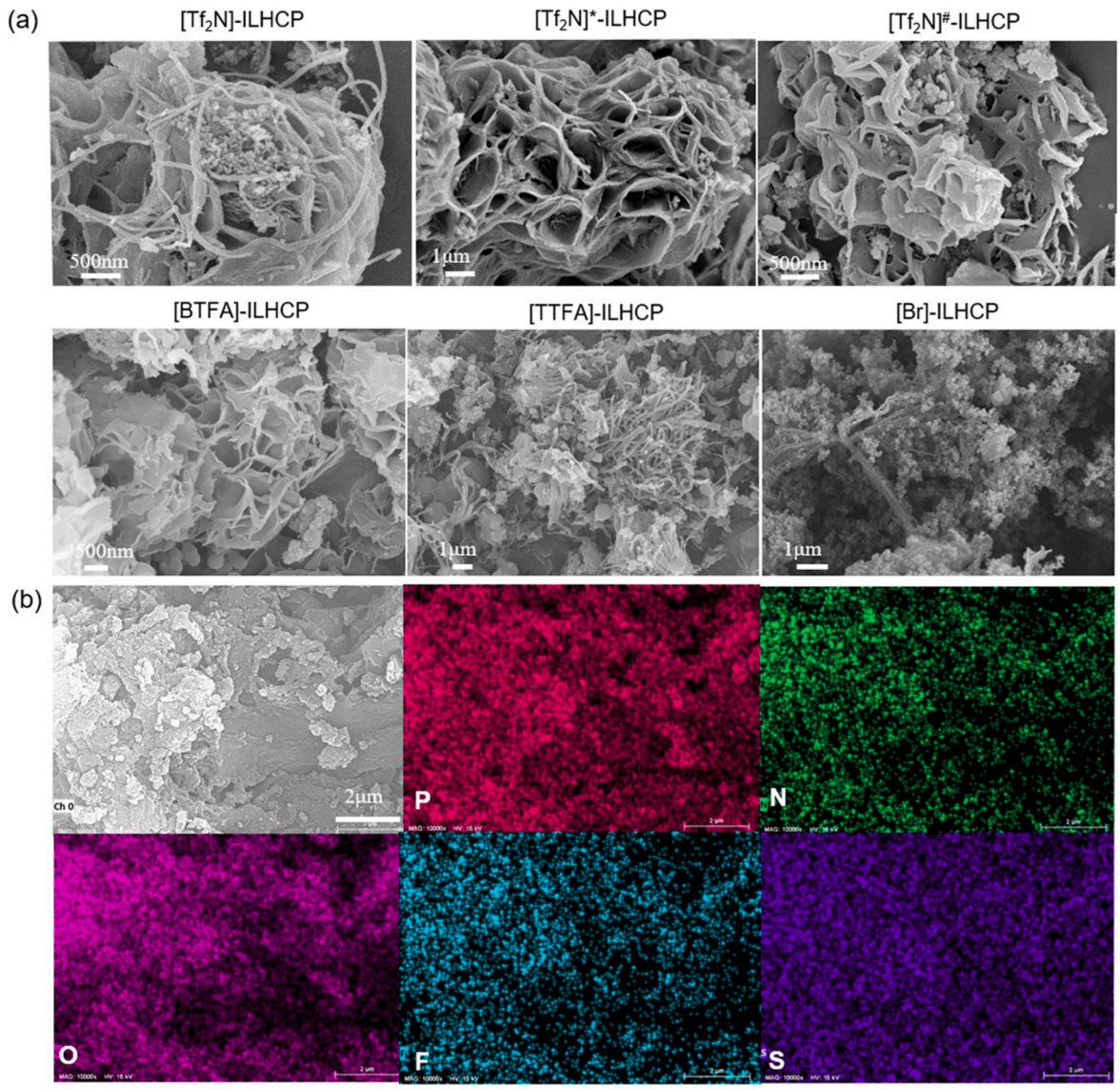

Fig. 4. (a) SEM images of ILHCPs, and (b) EDS mappings of [Tf_2N]-ILHCP.

Table 2
Element analysis (in wt%) and IL content (in mmol/g) of [Tf_2 N]-based HCPs.

HCP	Element analysis			IL content (calculated based on wt% S)
	C	H	S	
[Tf_2N]-ILHCP	73.80	4.28	1.68	0.262
[Tf_2N]*-ILHCP	73.08	4.13	1.36	0.212
[Tf_2N]$^{\#}$-ILHCP	65.22	3.83	1.30	0.203

2.3. Synthesis of ILHCPs

Six ILHCPs used in this work were synthesized from ILs and DCX following pre-synthesis methods [65]. Take the synthesis of [TF_2N]-ILHCP as an example. The reactants, [Ph_4P][Tf_2N] (3.0977 g, 5 mmol) and DCX (0.8753 g, 5 mmol), were added in DCE (70 ml) with anhydrous $FeCl_3$ (3.242 g, 20 mmol) as the catalyst. After the reflux reaction at 80 °C under N_2 atmosphere for 24 h, the brown precipitate was collected and washed with ethanol and water until the wash solution is colorless and clear. [Tf_2N]-ILHCP was readily obtained after drying the crude product in a vacuum drying oven at 120 °C for 24 h. Other ILHCPs were obtained using different initial molar ratio between the IL and the building block (DCX) by the same way (Fig. 1).

2.4. Characterization of ILHCPs

The N_2 adsorption–desorption isotherms, pore size distributions, and Brunauer-Emmett Teller (BET) surface areas of all ILHCPs were measured at 77 K on Micromeritics ASAP 2460. The total pore volumes and the micropore volumes were obtained from the N_2 adsorption–desorption isotherms. The average pore sizes and pore size distributions were calculated from the adsorption branches by the non-local density functional theory (NLDFT) method. The surface morphologies and microstructures of ILHCPs were analyzed by Scanning Electron Microscope (SEM, Gemini 500). The Elemental analysis was conducted using elemental analyzer (Thermo Fisher Scientific Flash 2000). Fourier transform infrared (FT-IR) spectra of ILHCPs were measured on Thermo Scientific Nicolet iS20. Solid state ^{13}C CPMAS NMR (Bruker 400 M) were obtained at ambient temperature. The thermal stabilities of ILHCPs were carried out by using a thermogravimetric analysis (TGA, Netzsch TG 209 F3 Tarsus) in N_2 atmosphere with a heating rate of 10 °C min^{-1}. The water contact angles were measured using an automatic video contact angle tester (Chengde JY-82C). X-ray photoelectron spectroscopy (XPS) was used to study the surface element composition and bond energy

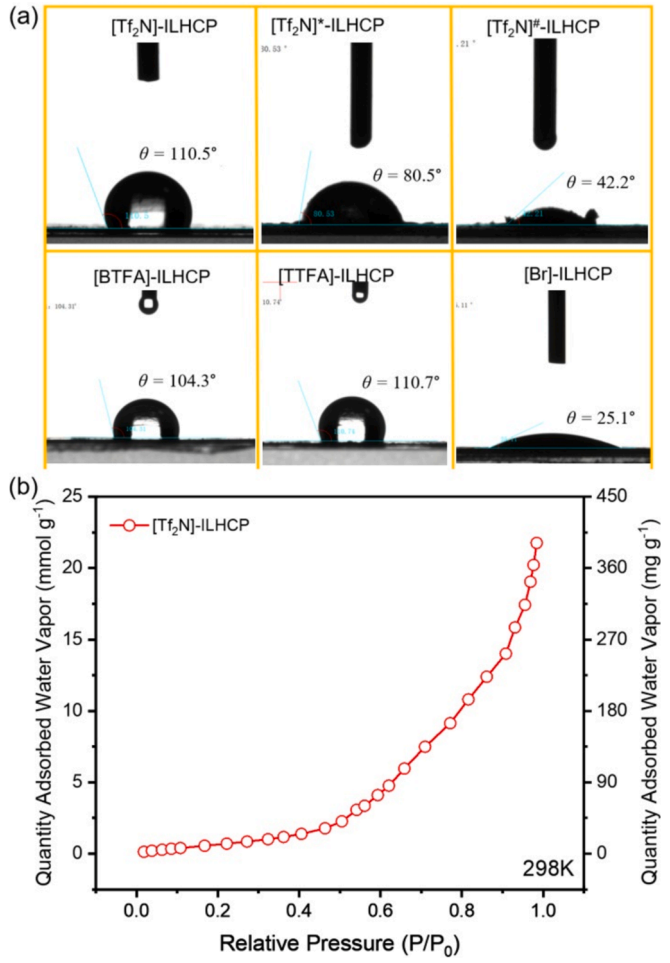

Fig. 5. (a) Water contact angles (θ, in °) of ILHCPs, and (b) water vapor adsorption on [Tf_2N]-ILHCP at 298 K.

analysis of samples by Thermo Fisher Scientific K-alpha + equipped with Al K radiation (1486.68 eV). Prior to conducting measurements, each sample underwent activation at 120°C under reduced pressure for a duration of 3 h to eliminate any adsorbed water and gases.

2.5. Gaseous toluene adsorption

The gaseous toluene adsorption isotherms on the ILHCPs were measured at 298, 308, and 318 K on Micromeritics ASAP 2460.The maximum adsorption pressure reached the saturated vapor pressure at it measured temperature.The model about Dual-Site Langmuir-Freundlich (DSLF) [67] as follows was used to describe the gaseous toluene adsorption on two different adsorption sites in the ILHCPs:

$$q_e = \frac{q_1 \times k_1 \times P^{\frac{1}{n_1}}}{1 + k_1 \times P^{\frac{1}{n_1}}} + \frac{q_2 \times k_2 \times P^{\frac{1}{n_2}}}{1 + k_2 \times P^{\frac{1}{n_2}}}$$

where q_e in mmol/g is the equilibrium adsorption capacity; q_1 and q_2 in mmol/g are the saturated adsorption capacities of adsorption sites 1 and 2, respectively; n_1 and n_2 are dimensionless constants representing the heterogeneity of the surface; k_1 (in $kPa^{-1/n1}$) and k_2 (in $kPa^{-1/n2}$) are the affinity coefficients of site 1 and 2, respectively; P in kPa is the pressure of bulk gas equilibrated with the adsorbed phase. Thus, two separated isotherms of site 1 and site 2 were fitted by the following equations, respectively,

$$q_{e,1} = \frac{q_1 \times k_1 \times P^{\frac{1}{n_1}}}{1 + k_1 \times P^{\frac{1}{n_1}}}$$

$$q_{e,2} = \frac{q_2 \times k_2 \times P^{\frac{1}{n_2}}}{1 + k_2 \times P^{\frac{1}{n_2}}}$$

where $q_{e,1}$ and $q_{e,2}$ in mmol/g is the equilibrium adsorption capacity of site 1 and site 2, respectively.

Breakthrough experiments were used to analysis the effect of relative humidity on the adsorption of gaseous toluene on the ILHCPs (Fig. 2). The breakthrough experiment was conducted using a custom-designed gas chromatography (GC, Agilent 8860 GC) workstation for the laboratory. Briefly, the mixture of gaseous toluene and water vapor with carrier gas of air was flowed to the U-tube and the toluene concentration was fixed at about 2000 ppm. The concentration of toluene in the outlet stream was measured and recorded by GC equipped with hydrogen flame ionization detector (FID). The capacities about equilibrium adsorption (q_e, in mg g^{-1}) were the maximum adsorption capacities when the ILHCPs stopped adsorption, and q_e could be calculated according to the following equation [68]:

$$q_e = \frac{F \times C_0 \times 10^{-6}}{W}[t_s - \int_0^{t_s} \frac{C_i}{C_0} dt]$$

where F in ml min^{-1} is the total flow rate ($F = 30$ ml min^{-1}), t in min is adsorption time, t_s in min is the equilibrium time, C_0 in mg m^{-3} is the concentration of toluene in the feed gas stream, C_i in mg m^{-3} is the concentration of toluene in the exit gas stream at $t = i$, and W in gram is the adsorbent weight. The reversible adsorption performances were tested as follows: dynamic adsorptions of 2000 ppm gaseous toluene with relative humidity 80 % in a typical ILHCP were tested for 180 mins under 25 °C (stopped before saturation for efficiency consideration), desorptions of toluene-saturated ILHCP were tested at 60 °C under N_2 until equilibrium was reached.

2.6. Isosteric heat of gaseous toluene adsorption

The isosteric heats of gaseous toluene adsorption (Q_{st}, in kJ mol^{-1}), for estimating the strength of adsorption interaction between toluene molecules and the ILHCP surface, according to the adsorption isotherms of gaseous toluene at 298, 308 and 318 K, the indefinite integral formula of the Clausius-Claperon equation is used to calculate:

$$\ln p = \frac{Q_{st}}{RT} + C$$

Where p (bar) and T (K) represent the pressure and corresponding temperature when the adsorption amount is fixed, R is the gas constant, 8.314 J mol^{-1} K^{-1}, and C is a constant. Q_{st} can be obtained from the slope of the linear curve of $\ln p$ to $1/T$ (in 1/K) at the same adsorption capacity.

2.7. Calculation of selectivity

The selectivity of gaseous toluene / water vapor was calculated to identify the separation efficiency with the following equation [69]:

$$S_{toluene/water} = \frac{m_{toluene}}{m_{water}}$$

where $m_{toluene}$ and m_{water} denote the saturated concentrations of gaseous toluene and water vapor in the ILHCP in the unit of mmol/g at 298 K under different partial of toluene and water, respectively. $S_{toluene/water}$ are utilized to estimate the capability of ILHCPs for selective separation of toluene from water.

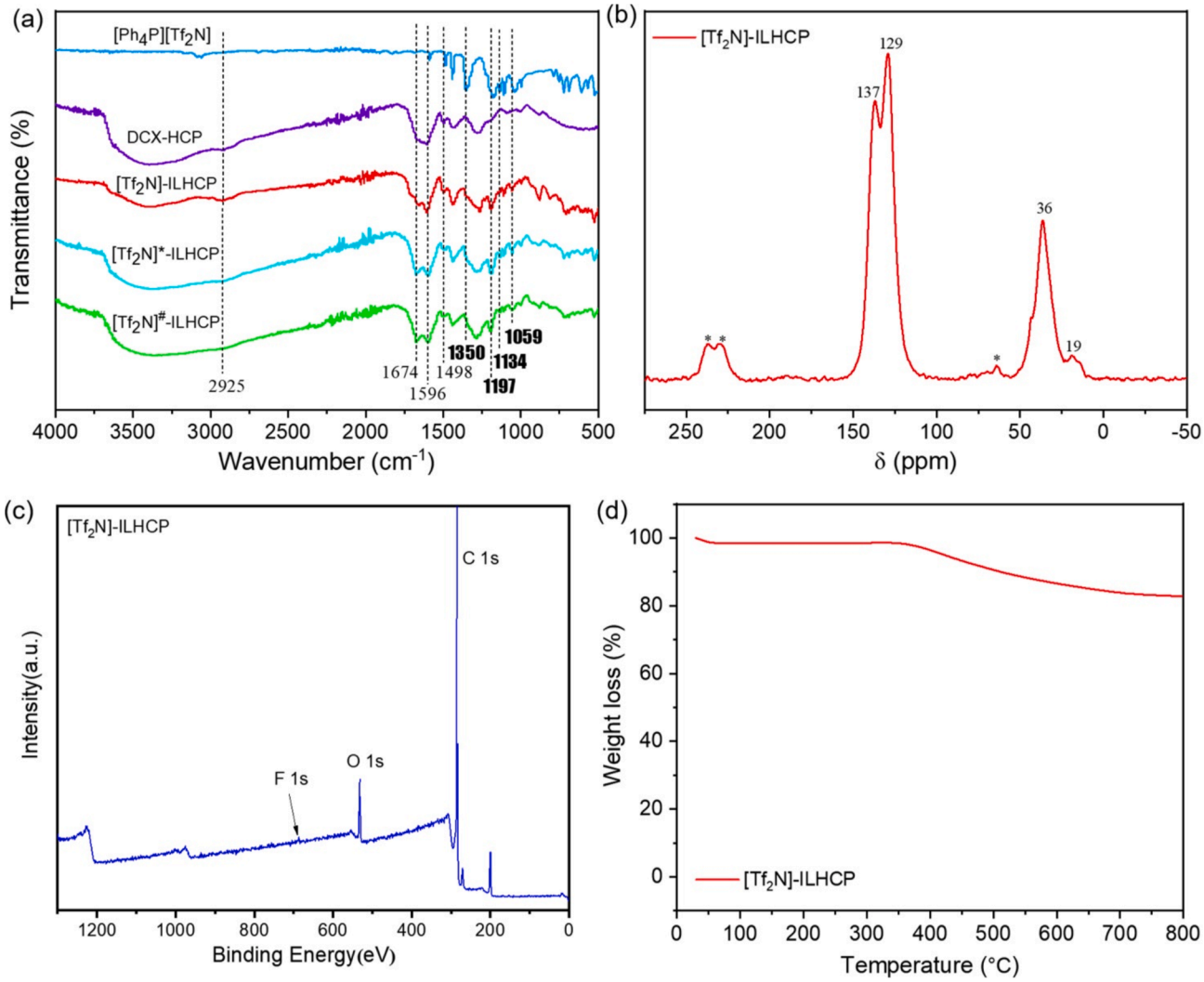

Fig. 6. (a) Comparison of FT-IR spectra of $[Ph_4P][Tf_2N]$-embedded ILHCPs and corresponding IL $[Ph_4P][Tf_2N]$; (b) Solid-state ^{13}C CP/MAS NMR spectrum; (c) XPS spectrum; and (d) TGA curve of $[Tf_2N]$-ILHCP.

3. Results and discussion

3.1. Physical characteristics

N_2 adsorption–desorption isotherms at 77 K of these ILHCPs are shown in Fig. 3, and the corresponding surface area, pore volume, and pore size are collected in Table 1. There is a sharp increase up to 200 cm^3 g^{-1} at low relative pressure ($P/P_0 < 0.01$), indicating the abundant micropores in ILHCPs, while a slow increase could be seen during the relative pressure in the range from 0.01 to 0.9, indicating the presence of mesopores. N_2 adsorption increased rapidly at high relative pressure ($P/P_0 > 0.9$), indicating the presence of cleavage-sheet pores. These results suggested the hierarchical pore structures of these ILHCPs, and the presence of micropores provided and advantage for gas adsorption. Based on the classification by the International Union of Pure and Applied Chemistry (IUPAC),the N_2 adsorption–desorption isotherms showed type II shape with an type H3 hysteresis loop, suggesting the formation of non-rigid structure [70]. BET surface areas (S_{BET}) of 772.5, 909.9, 612.9, 429.1, 318.8 and 735.2 m^2 g^{-1} could be obtained by $[Tf_2N]$-ILHCP, $[Tf_2N]$*-ILHCP, $[Tf_2N]^{\#}$-ILHCP, [BTFA]-ILHCP, [TTFA]-ILHCP, and [Br]-ILHCP respectively. Additionally, the total pore volume (V_{tot}) decreased from 0.93 to 0.63 cm^3 g^{-1} with decreased IL:DCX molar ratio from 5:5 to 1:5. Besides, the micropore volume (V_{mic}) of ILHCP-$[Tf_2N]$-ILHCP, $[Tf_2N]$*-ILHCP, and $[Tf_2N]^{\#}$-ILHCP are 0.17, 0.32, and 0.20 cm^3 g^{-1}, indicating that more IL moieties in ILHCPs are not conducive to the formation of micropores. Thus, the values of V_{mic} decreased with the order $[Tf_2N]$*-ILHCP > $[Tf_2N]^{\#}$-ILHCP > $[Tf_2N]$-ILHCP, and the reverse order could be found for the average pore size (D): $[Tf_2N]$*-ILHCP (3.8 nm) < $[Tf_2N]^{\#}$-ILHCP (4.1 nm) < $[Tf_2N]$-ILHCP (4.8 nm). These results suggested that although more and more ILs in ILHCPs could increase the values of D and V_{tot}, the value of V_{mic} was decreased, which may affect the adsorption performance. The average pore size of [BTFA]-ILHCP (8.2 nm) and [TTFA]-ILHCP (9.8 nm) are different than other ILHCPs, probably because of the large anions.

The morphology of ILHCPs including $[Tf_2N]$-ILHCP, $[Tf_2N]$*-ILHCP, $[Tf_2N]^{\#}$-ILHCP, [BTFA]-ILHCP, [TTFA]-ILHCP, and [Br]-ILHCP were investigated by scanning electron microscopy (SEM) and the results were collected. As shown in Fig. 4(a), SEM image of ILHCPs shows a porous amorphous bulk structure. For $[Tf_2N]$-based ILHCPs, the SEM images showed that the ILHCPs were irregular layers, resulting in the high specific surface area [71], While the [BTFA]-ILHCP morphology becomes filled with sheet-like structures and amorphous bulks, there is a notable reduction in specific surface area [72,73]. Specially, SEM image showed the irregular fiber-like structure of [TTFA]-ILHCP, which also leads to the decreased specific surface area [74]. Among these ILHCPs, the SEM image of [Br]-ILHCP shows a more developed porous amorphous structure, indicating the increased specific surface area [72]. All these results indicated that different anions lead to different

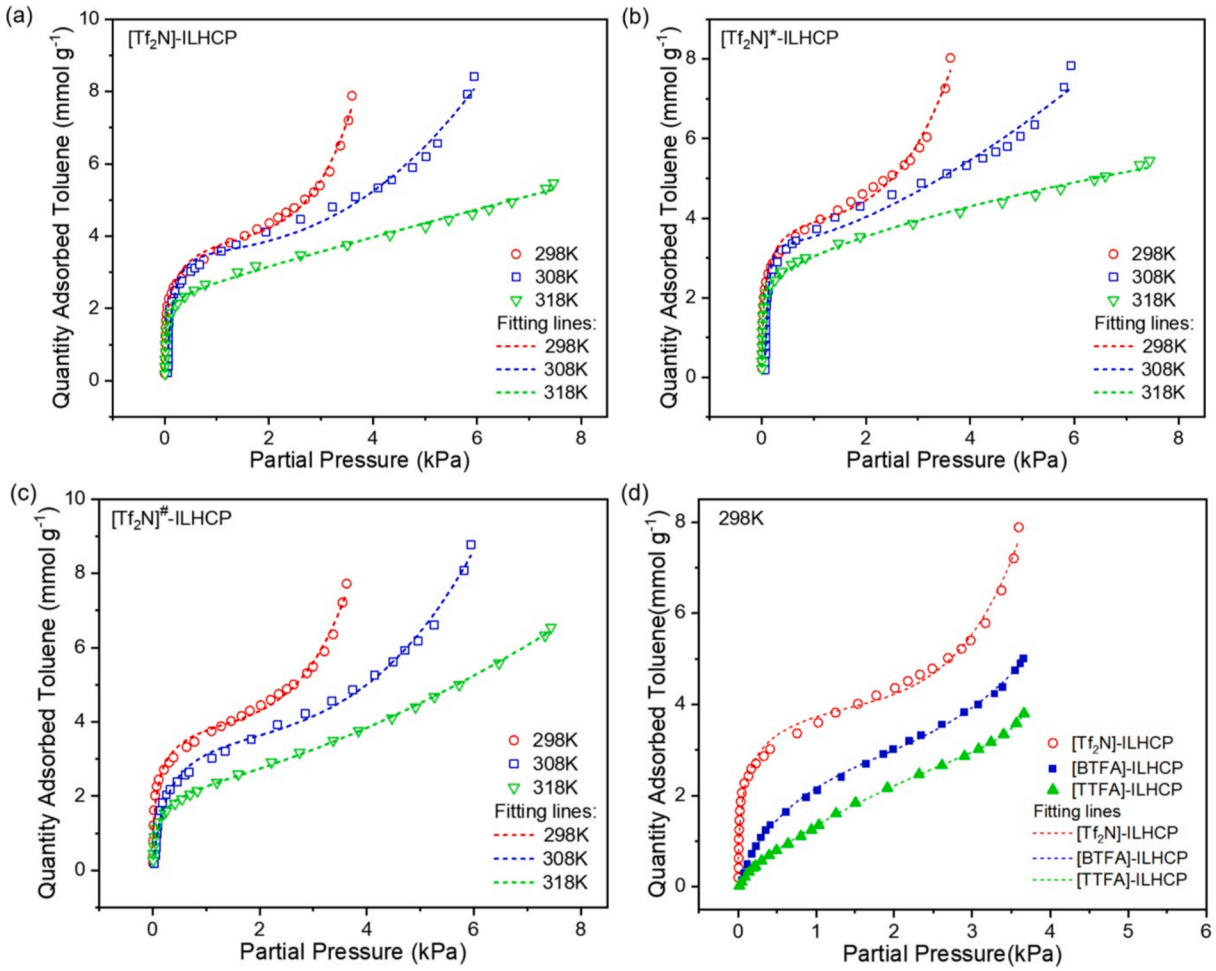

Fig. 7. Adsorption isotherms of gaseous toluene on the ILHCPs.

Table 3
Fitting parameters of DSLF equation (T in K, q_1 and q_2 in mmol/g, k_1 in $kPa^{-1/n1}$ and k_2 in $kPa^{-1/n2}$, n_1 and n_2 are dimensionless).

ILHCP	T	Site 1			Site 2			R^2
		q_1	k_1	$1/n_1$	q_2	k_2	$1/n_2$	
$[Tf_2N]$-ILHCP	298	5.04	2.80	0.53	30.25	1.81×10^{-4}	5.00	0.990
	308	3.65	24.99	1.57	203.49	2.29×10^{-4}	2.56	0.979
	318	2.28	47.65	1.09	1138.69	4.18×10^{-4}	0.92	0.996
$[Tf_2N]$*-ILHCP	298	4.43	6.81	0.74	67.33	4.05×10^{-4}	3.78	0.989
	308	3.29	905.56	3.05	5488.99	4.60×10^{-5}	1.55	0.983
	318	2.08	453.61	1.44	937.68	0.0010	0.61	0.997
$[Tf_2N]^{\#}$-ILHCP	298	4.83	3.51	0.60	10.81	0.0010	4.40	0.990
	308	4.12	3.05	0.92	5.81	0.0021	3.34	0.994
	318	2.69	3.70	0.65	14.80	0.010	1.66	0.999

morphologies with different porous structures. Additionally, the EDS mappings of $[Tf_2N]$-ILHCP, illustrated in Fig. 4(b), exhibited that P, N, O, F, and S elements were contained, indicating the successful synthesis of ILHCPs.

Elemental analysis was further applied to calculate the contents of IL in typical $[Ph_4P][Tf_2N]$-embedded ILHCPs, and the results were also listed in Table 2. The S contents in these ILHCPs were 1.68 %, 1.36 %, and 1.30 % for $[Tf_2N]$-ILHCP, $[Tf_2N]$*-ILHCP, $[Tf_2N]^{\#}$-ILHCP, respectively. Thus, the contents of $[Ph_4P][Tf_2N]$ were calculated to be 0.262, 0.212, and 0.203 mmol g^{-1}. The loading of $[Ph_4P][Tf_2N]$ decreased with the order $[Tf_2N]$-ILHCP > $[Tf_2N]$*-ILHCP > $[Tf_2N]^{\#}$-ILHCP, originating from the quantity of IL used during the synthesis was increased in the initial molar composition of these ILHCPs ($[Ph_4P][Tf_2N]$: DCX) from 5 mmol: 5 mmol, to 3 mmol: 5 mmol and 1 mmol: 5 mmol for $[Tf_2N]$-ILHCP, $[Tf_2N]$*-ILHCP, $[Tf_2N]^{\#}$-ILHCP, respectively.

Besides, to determine the hydrophobicity property, the water contact angles (θ, in °) for ILHCPs were measured to be 110.5°, 80.5°, 42.2°, 104.3°, 110.7°, and 25.1° for $[Tf_2N]$-ILHCP, $[Tf_2N]$*-ILHCP, $[Tf_2N]^{\#}$-ILHCP, [BTFA]-ILHCP, [TTFA]-ILHCP, and [Br]-ILHCP, respectively (Fig. 5a). The results indicated that the $[Tf_2N]$-ILHCP, [BTFA]-ILHCP, and [TTFA]-ILHCP, are more hydrophobic than other ILHCPs, especially [Br]-ILHCP. Moreover, the values of water contact angles

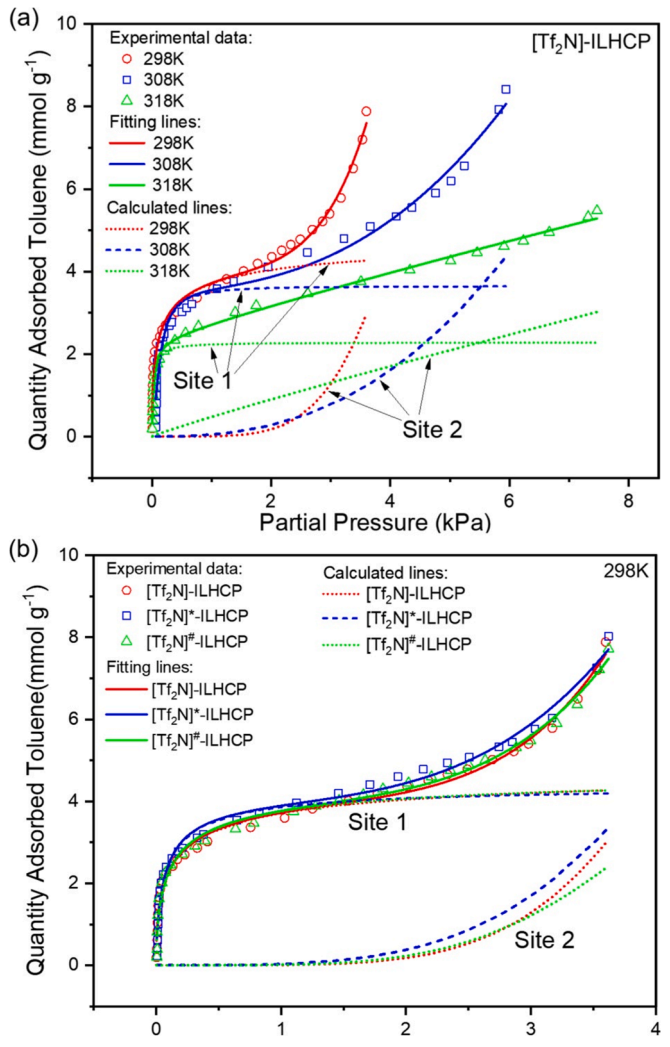

Fig. 8. Decomposed gaseous toluene isotherms of the [Ph_4P][Tf_2N]-embedded ILHCPs from two sites of the DSLF model. (a) [Tf_2N]-ILHCP under different temperatures. (b) different [Ph_4P][Tf_2N]-embedded ILHCPs under 298 K.

decreased with the order [Tf_2N]-ILHCP > [Tf_2N]*-ILHCP > [Tf_2N]$^{\#}$-ILHCP, indicating that hydrophobicity decrease with the decreased content of [Ph_4P][Tf_2N] in ILHCPs. Additionally, water vapor adsorption isotherm of [Tf_2N]-ILHCP at 298 K was measured, and the result was illustrated in Fig. 5b and Table S1. It showed that the synthesized [Tf_2N]-ILHCP demonstrated a reduced absorption of water vapor, and this value progressively rose as the water vapor pressure increased, suggesting a characteristic of physisorption.

FT-IR and ^{13}C solid-state NMR spectra were measured to further verify the successful synthesis of ILHCPs (Fig. 6). The comparison of FT-IR spectra of ILHCPs ([Tf_2N]-ILHCP, [Tf_2N]*-ILHCP, [Tf_2N]$^{\#}$-ILHCP) with that of ILs ([Ph_4P][Tf_2N]) and DCX-HCP are shown in Fig. 6a. The FT-IR spectra of these HCPs exhibited a series of typical stretching vibrations of the skeletal benzene ring at 1498, 1596, and 1674 cm^{-1}. Another new characteristic peak observed at 2925 cm^{-1} could be assigned to the C–H bending vibration of methylene group (−CH_2−) between two benzene rings in the skeleton, originating from DCE. Compared with the FT-IR spectra of HCP-DCX and [Ph_4P][Tf_2N], a vibration at 1350 and 1134 cm^{-1} in the spectra of [Ph_4P][Tf_2N]-embedded ILHCPs could be assigned to asymmetric stretching and symmetric vibration of S = O bonds, respectively, while new bonds at 1059 and 1197 cm^{-1} could be assigned to stretching vibrations of −SNS− and −CF_3 bonds, respectively [75]. The solid-state ^{13}C CP/MAS NMR spectrum of [Tf_2N]-ILHCP is illustrated in Fig. 6b. The signal peaks

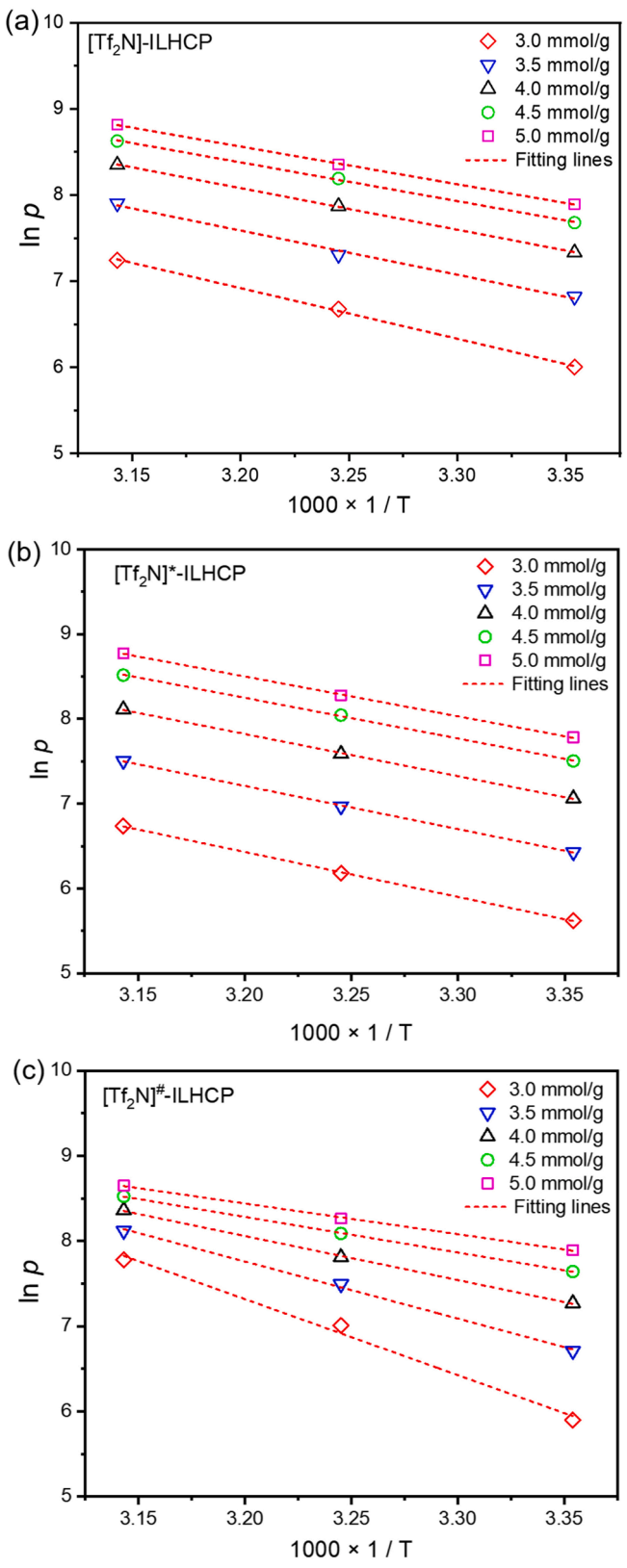

Fig. 9. ln$p$ versus 1/T for estimation of isosteric adsorption heats of gaseous toluene on the ILHCPs.

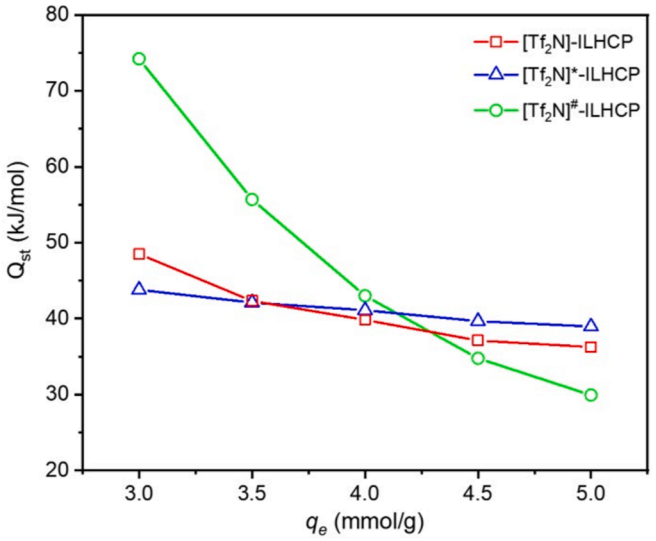

Fig. 10. Isosteric heat of gaseous toluene adsorption on the ILHCPs as a function of toluene amounts adsorbed.

at 137 and 129 ppm could be assigned to the substituted and non-substituted aromatic carbons in the structure, respectively, while the resonance peaks at 36 and 19 ppm due to the carbon in the methylene linkers (−CH_2 −) and carbon in the end chloromethyl (−CH_2Cl). The shifts with asterisks in the spectra donate spinning sidebands [76]. XPS survey spectra of [Tf_2N]-ILHCP are provided in Fig. 6c. The characteristics peaks of C 1s, O 1s and F 1s are found at 282.1, 532.1, and 688.1 eV, respectively, in full survey XPS spectra. Thus, based on the analysis, ILHCPs were successfully synthesized for gaseous toluene adsorption. TGA was performed to test the thermal stability of [Tf_2N]-ILHCP (Fig. 6d). The mass loss between room temperature to100 °C assigned to the evaporation of water and removal the impurities on the surface and pore structures. At temperatures below 300 °C, the mass loss of ILHCPs is within 10 %, suggesting the excellent thermal stability.

3.2. Adsorption of gaseous toluene

3.2.1. Gaseous toluene adsorption isotherms

The adsorption isotherms of gaseous toluene on the HCPs embedded with different kinds of ILs, including [Tf_2N]-ILHCP, [Tf_2N]*-ILHCP, [Tf_2N]$^{\#}$-ILHCP, [BTFA]-ILHCP, and [TTFA]-ILHCP, were measured, and the results were illustrated in Fig. 7. Clearly, although the water contact angles (θ, in °) for [Tf_2N]-ILHCP (110.5°), [BTFA]-ILHCP (104.3°), and [TTFA]-ILHCP (110.7°) were measured to be similar, the adsorption capacities of gaseous toluene by these ILHCPs were measured to be at 2.65, 0.83, and 0.42 mmol, respectively, at 298 K and 2000 ppm (0.2 kPa), indicating that the reason for different adsorption capacities probably stem from the different structures of anions. Moreover, the adsorption capacities of gaseous toluene by all these ILHCPs decreased with the increase of temperature while they increased with the increase of partial pressure. Besides, a two-step rise is observed in these adsorption isotherms up to the saturated toluene vapor pressure at the desired temperature, with a more pronounced trend evident at lower temperatures. The initial sharp increase occurs at low pressure, which can be attributed to a strong affinity for toluene due to π-π interactions with the benzene rings within the channels of the ILHCPs network. Subsequently, the gaseous toluene adsorption capacities approach a plateau, followed by a slight increase until reaching the saturated toluene vapor pressure, which is related to pore condensation at high pressure. Additionally, gaseous toluene adsorption isotherms of these ILHCPs are similar, indicating they are all suitable for efficient gaseous toluene adsorption under dry conditions. Furthermore, the isotherms on these ILHCPs could be fitted with DSLF model. The fitted results are illustrated in Fig. 7, while the fitting parameters for sites 1 and 2 are presented in Table 3. The fitting results demonstrate a strong agreement with the experimental data ($R^2 > 0.9$). Two distinct isotherms for site 1 and site 2 are shown in Fig. 8. Notably, the capacity and affinity coefficient of site 1 decreased with increasing temperature, suggesting that the π-π interactions gradually weakened as the temperature rose. In contrast, the capacity of site 2 ultimately increased, attributed to capillary condensation occurring within the pores.

3.2.2. Isosteric heat of gaseous toluene adsorption

Isosteric heats (Q_{st}, in kJ/mol) have been calculated from the slope of the linear plot of ln$p$ against $1/T$ at the same adsorbed quantity from gaseous toluene adsorption isotherms utilizing the indefinite integral formula of the Clausius-Clapeyron equation. The linear relationship of ln$p$ *vs* $1/T$ was showed in Fig. 9 while isosteric heats of gaseous toluene adsorptions on the ILHCPs *vs* the adsorbed amount of toluene (q_e, in mmol/g) were illustrated in Fig. 10. The results showed that owing to the surface heterogeneity, the isosteric heats of adsorption on [Tf_2N]$^{\#}$-ILHCP declined from 70 to 30 kJ/mol with increasing amount adsorbed toluene from 3 to 5 mmol g^{-1}. The results suggest that toluene could be adsorbed relatively easily within the low adsorption capacity, while toluene need to transfer to relatively inaccessible sites in the interior pores within the high adsorption capacity, leading to the decreased isosteric heats. For [Tf_2N]*-ILHCP, the isosteric heats of toluene adsorption were in the small range of 39 ~ 44 kJ/mol with increasing amount adsorbed toluene, ascribing to the energetically homogeneous surface of the [Tf_2N]*-ILHCP. Compared with the adsorption on [Tf_2N]$^{\#}$-ILHCP, the possible reasons were adding more [Ph_4P][Tf_2N] in the networks of [Tf_2N]*-ILHCP increased the π-π interaction as well as the more micropore volume enhanced the affinity towards toluene. For [Tf_2N]-ILHCP, the largest amount of [Ph_4P][Tf_2N] resulted in the enhanced average pore size and increased the surface energetical heterogeneity.

3.3. Breakthrough experiments under relative humidity

In order to discuss the selective separation of toluene form water, we first calculated the $S_{toluene/water}$ for [Tf_2N]-ILHCP, according to the Fig. 7a and Table S1. The results showed that the $S_{toluene/water}$ of 2000 ppm (0.2 kPa) toluene under different humidity were calculated to be 0.13, 0.26, 0.62, 2.64, and 4.37 for relative humidities (RH) of 100, 80, 60, 40 and 20 %, respectively, indicating the selectivity increased with the decrease of humidity. Thus, the breakthrough experiments of gaseous toluene adsorption at 298 K by [Ph_4P][Tf_2N]-embedded ILHCPs ([Tf_2N]-ILHCP, [Tf_2N]*-ILHCP, [Tf_2N]$^{\#}$-ILHCP) and DCX-HCP under relative humidities (RH) of 0, 40, 60, and 80 % with the gas concentration of 2000 ppm at the inlet were performed, and the breakthrough curves were showed in Fig. 11. The equilibrium adsorption capacities (q_e, in mg g^{-1}) were calculated *via* integrating the breakthrough curves from $t = 0$ to equilibrium time ($t = t_e$), and the results were also listed in Table 4. It is clearly seen that [Tf_2N]-ILHCP, [Tf_2N]*-ILHCP, and [Tf_2N]$^{\#}$-ILHCP possessed lower toluene uptakes than DCX-HCP in dry atmosphere. As DCX-HCP was more hydrophilic, water molecules would more readily occupy the cavities due to hydrogen bonding. Moreover, as humidity rose, the breakthrough time of toluene vapor on the DCX-HCP decreased, indicating a significant reduction in adsorption capacity with higher moisture levels. For [Ph_4P][Tf_2N]-embedded ILHCPs, especially [Tf_2N]-ILHCP embedded with more [Ph_4P][Tf_2N] molecules, the breakthrough time of toluene vapor on ILHCP is mainly steady (~ 270 mg g^{-1}) when relative humidities (RH) increase from 40 to 80 %. As the initial molar ratio of IL:DCX for synthesis [Ph_4P][Tf_2N]-embedded ILHCPs increased from 1:5 to 5:5, the toluene adsorption capacity increased from 251mg g^{-1} for [Tf_2N]$^{\#}$-ILHCP to 276 mg g^{-1} for [Tf_2N]*-ILHCP at 298 K under RH = 80 %, while decreased to 266 mg g^{-1} for [Tf_2N]-ILHCP, probably because of the BET surface areas (S_{BET}) of these

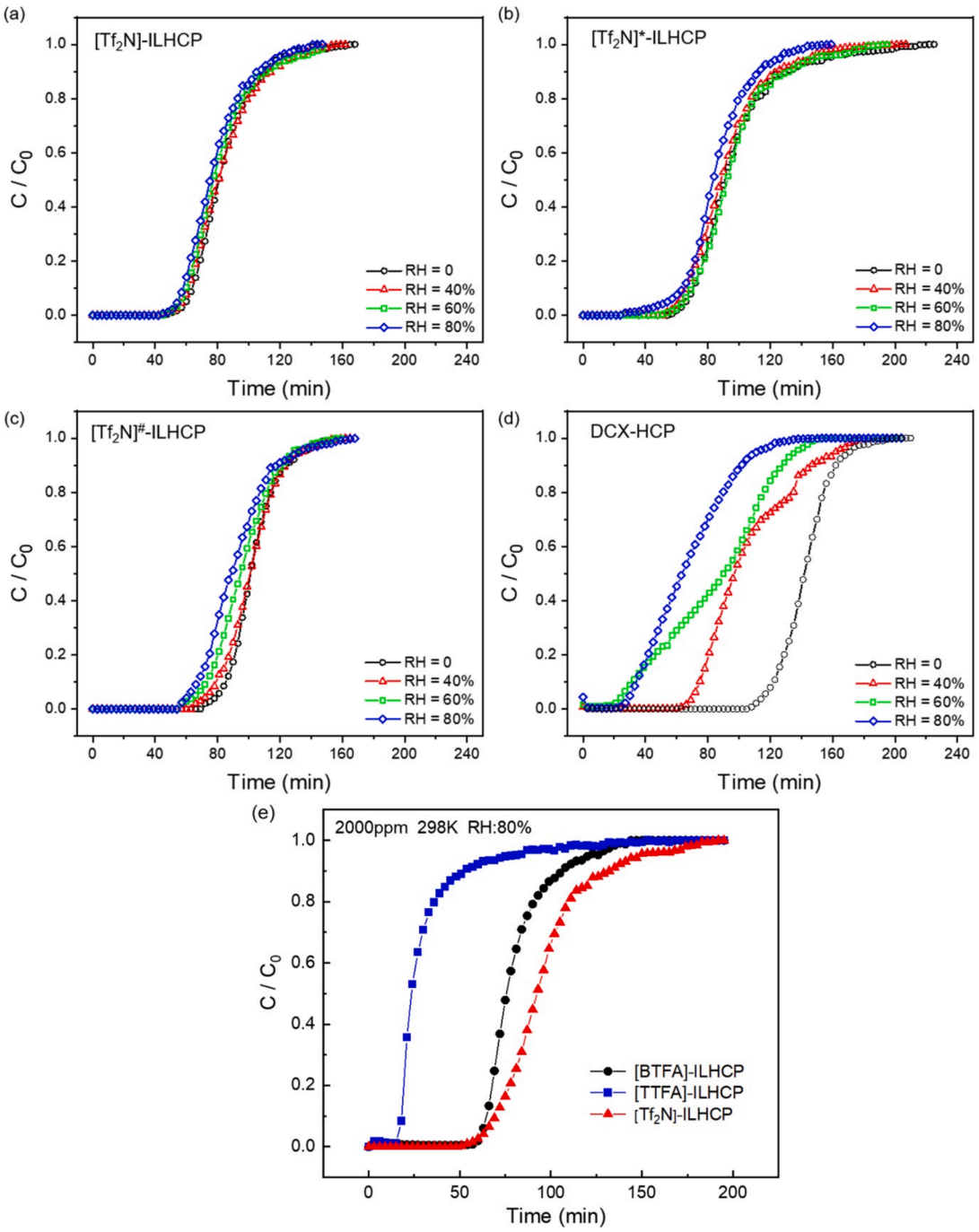

Fig. 11. Effect of relative humidity (a-d) and structures of anions (e) on the gaseous toluene breakthrough curves at 298 K with the gas concentration of 2000 ppm at the inlet.

Table 4
The equilibrium gaseous toluene adsorption capacities (q_e, in mg g^{-1}) of ILHCPs at 298 K under different relative humidities (RH) with the gas concentration of 2000 ppm at the inlet.

ILHCP	q_e, (mg g^{-1})			
	RH = 0	RH = 40 %	RH = 60 %	RH = 80 %
[Tf_2N]-ILHCP	271	271	266	266
[Tf_2N]*-ILHCP	306	305	296	276
[Tf_2N]$^{\#}$-ILHCP	283	271	261	251
HCP-DCX	350	266	214	170

ILHCPs first increased from 772.5 m^2 g^{-1}, for [Tf_2N]$^{\#}$-ILHCP to 909.9 m^2 g^{-1} for [Tf_2N]*-ILHCP and then decreased to 612.9 m^2 g^{-1} for [Tf_2N]-ILHCP. Consequently, these ILHCPs demonstrated a greater capacity to adsorb toluene than water vapor when compared to DCX-HCP in environments with high moisture levels. Furthermore, the breakthrough experiments of gaseous toluene adsorption by ILHCPs with different kinds of anions under RH = 80 % and 2000 ppm gaseous toluene conditions were also performed (Fig. 11e). The equilibrium adsorption capacities (q_e, in mg g^{-1}) were calculated to be 266, 218, 139 mg g^{-1} for [Tf_2N]-ILHCP, [BTFA]-ILHCP, and [TTFA]-ILHCP, respectively, from the breakthrough experiments. These results also indicated that the different structures of anions resulted in the different adsorption capacities. Moreover, the comparison of the toluene

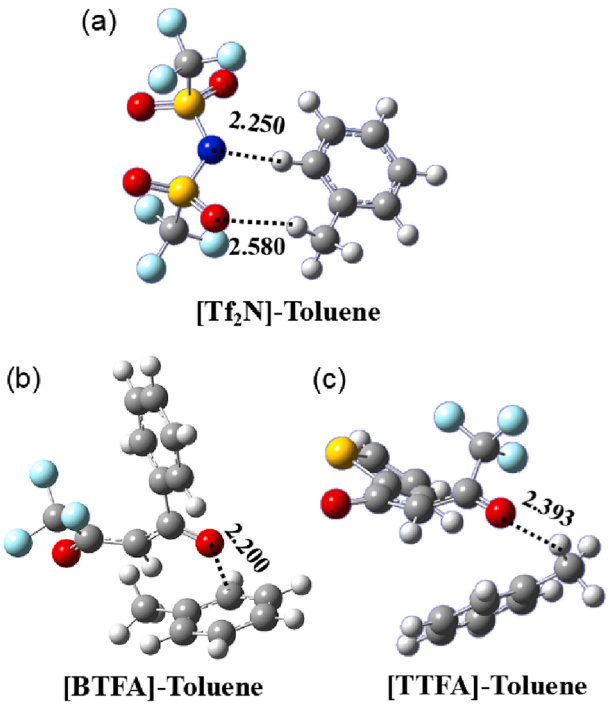

Fig. 12. Optimized structures of (a) [Tf_2N]-Toluene, (b) [BTFA]-Toluene, and (c) [TTFA]-Toluene showing the interactions between O atoms in the closest toluene molecules and the active sites in the anions. Note that the van der Waals radii [83] of atoms are 1.70 Å for C (gray), 1.20 Å for H (white), 1.52 Å for O (red), 1.55 Å for N (blue), 1.80 Å for S (yellow) and 1.47 Å for F(green), respectively. (For interpretation of the references to colour in this figure legend, the reader is referred to the web version of this article.)

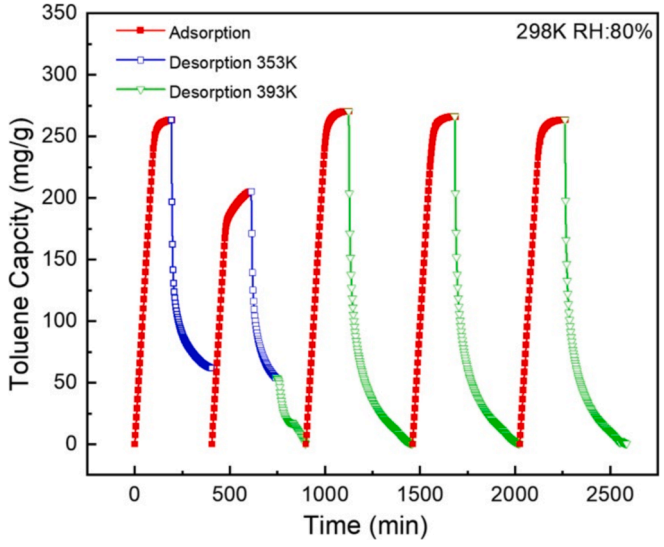

Fig. 13. Recycling performance of [Tf_2 N]-ILHCP for 5 successive reuses in toluene adsorption at 298 K and 2000 ppm toluene under 80 % relative humidities.

adsorption performance with other materials such as activated carbon or MOFs can be found in Table S2. It can be seen that 2.89 mmol/g (266 mg g^{-1}) gaseous toluene could be adsorbed by [Tf_2N]-ILHCP at 298 K under RH = 80 %, higher than most of other adsorbents. Although a kind of modified MIL-101 (D-MIL-101-20 %) was reported to adsorb 3.14 mmol/g gaseous toluene under same conditions [77], its $S_{toluene/water}$ is only 0.10, while that of [Tf_2N]-ILHCP is 0.26, indicating that D-MIL-101-20 % could also absorb water easily when absorbing toluene. Thus, ILHCPs is probably a kind of potential alternative adsorbents for toluene adsorption under humidity conditions.

3.4. Interaction of anions with toluene from quantum chemical calculations

Density functional theory (DFT) calculations are a helpful tool that could be used to study the mechanism of gaseous toluene adsorption. The distances between anions and toluene were calculated to identify the interactions using the Gaussian 16 Revision C.01 package [78] by DFT-D3(BJ)/B3LYP/6–31++G(d,p) methods [79–82]. Due to the key role of anions in gaseous toluene adsorption by ILHCPs, the structures of anion–toluene complexes were optimized, and the results were illustrated in Fig. 12. It can be seen that there are two interaction sites (negative charged N atom & O atom in C = O) in [Tf_2N]…toluene complex, while one interaction site in both [BTFA]…toluene (O atom in C = O) and [TTFA]…toluene (O atom in C = O) complexes. The intermolecular distance between negative charged N atom in [Tf_2N] anion and H atom in toluene was calculated to be 2.250 Å, corresponding to a reduction of 18.2 % of the sum of the van der Waals radii of the two interacting atoms. Thus, the results indicated the strong interaction of [Tf_2N]-embedded ILHCPs with gaseous toluene, resulting in the higher adsorption capacities of [Tf_2N]-embedded ILHCPs than [BTFA]-embedded ILHCP and [TTFA]-embedded ILHCP.

3.5. Stability and reversibility of the ILHCPs

Stability and reversibility are important properties of materials, which can be used to develop novel gas adsorbents. Fig. S1 illustrates the breakthrough experiments of gaseous toluene adsorption at 298 K under RH = 80 % with the gas concentration of 2000 ppm by [Tf_2N]-ILHCP with the comparison of adsorption by a kind of active carbon (AC-50) and a kind of MOF (CuBTC, synthesized according to the literature [84]) after same pre-treatment experiments, including 1 mol L^{-1} H_2SO_4 for 4 h (acid treatment), 1 mol L^{-1} NaOH for 4 h (alkali treatment), adsorption 1 % H_2O, and adsorption 5 % H_2O. The experiments of adsorption 1 % H_2O and adsorption 5 % H_2O were performed through samples exposing to humidity air at 288 K under RH = 80 % and completed when the absorption capacity of H_2O reached the requirements (Fig. S2). The equilibrium adsorption capacities (q_e, in mg g^{-1}) were listed in Table S3. It can be seen that about 240 mg g^{-1} gaseous toluene could be obtained by [Tf_2N]-ILHCP whether after acid treatment or alkali treatment, while there is a significant difference in toluene capacities of AC-50 and CuBTC, indicating a significant influence for AC-50 and CuBTC by acid treatment and alkali treatment. When added 1 % H_2O and 5 % H_2O in [Tf_2N]-ILHCP, AC-50, and CuBTC. Although the differences of toluene capacities between the [Tf_2N]-ILHCP and AC-50 were not significant when added 1 % H_2O or 5 % H_2O, [Tf_2N]-ILHCP has significant advantage compared with AC-50 because of the lower water adsorption of [Tf_2N]-ILHCP (10.9 % in weight ratio) than AC-50 (30.7 % in weight ratio) (Fig. S2). The desorption performance and the adsorption–desorption reversible cycles for [Tf_2N]-ILHCP are shown in Fig. 13. It can be seen that the first toluene adsorption of [Tf_2N]-ILHCP was 263 mg g^{-1} at 298 K under RH = 80 % and 2000 ppm toluene concentration. After the first desorption at 353 K, the second adsorption capacity decreased significantly to 205 mg g^{-1}. Thus, high temperature needed to desorb the adsorbed toluene. It is clear that after the desorption performed at 393 K, the third adsorption capacity increased to 270 mg g^{-1} and maintained steady during the other cycles. Thereby, these results indicated the highly efficient and reversible gaseous toluene adsorption by hydrophobic ILHCPs under high humidity.

4. Conclusions

In summary, a strategy using ionic liquids embedded hyper-

crosslinked polymers (ILHCPs) for highly efficient gaseous toluene adsorption under high humidity has been developed. These ILHCPs with tunable hydrophobicity property could be obtained *via* anion-exchange and Friedel-Crafts reaction with 1,4-dichloroxylene (DCX) as the cross-linker. High surface area, high micropore volume, and small average pore size could be obtained through tuning the anion stuctures and the initial IL:DCX molar ratio. Gaseous toluene adsorption isotherms on typical ILHCPs were tested under 298, 308, and 318 K, and a dual-site Langmuir-Freundlich (DSLF) model was used for well describing adsorption isotherms, which can be divided into two contributions for site I and site II. The isosteric heats of gaseous toluene adsorption were calculated. Furthermore, toluene adsorption under different humidity conditions were also tested. Compared with DCX-based self-condensed HCP, toluene adsorption capacity of ILHCPs remained steadily, even under 80 % humidity. Based on the information we know so far, this is the first example of tuning functional ILHCPs for efficient H_2O-tolerant gaseous toluene adsorption. We believe that this method will open a door to achieving high adsorption efficiency of other volatile organic compounds (VOCs) or inorganic gases such as NO_x, SO_2, H_2S, and CO_2 by functional IL-based porous organic polymers (POPs).

CRediT authorship contribution statement

Xiongfei Nie: Visualization, Investigation, Data curation. **Xinjie Qiu:** Validation, Investigation, Data curation. **Ruina Zhang:** Visualization, Methodology, Data curation. **Quanli Ke:** Funding acquisition, Formal analysis. **Huayan Liu:** Methodology, Formal analysis. **Xiangping Zhang:** Resources, Formal analysis. **Hanfeng Lu:** Resources, Project administration, Funding acquisition, Conceptualization. **Guokai Cui:** Writing – review & editing, Writing – original draft, Supervision, Project administration, Investigation, Funding acquisition, Conceptualization. **Suojiang Zhang:** Formal analysis, Conceptualization.

Declaration of competing interest

The authors declare that they have no known competing financial interests or personal relationships that could have appeared to influence the work reported in this paper.

Acknowledgements

This work was financially supported by the National Natural Science Foundation of China (Nos. 22078294, 22378353, 22208300), the Key Research and Development Project in Zhejiang Province (Nos. 2024C03108, 2023C03127, 2024C03114), and the Zhejiang Provincial Postdoctoral Science Foundation (No. ZJ2023145).

Appendix A. Supplementary data

Supplementary data to this article can be found online at https://doi.org/10.1016/j.cej.2025.159467.

Data availability

Data will be made available on request.

References

[1] W. Zhang, G. Li, H. Yin, K. Zhao, H. Zhao, T. An, Adsorption and desorption mechanism of aromatic VOCs onto porous carbon adsorbents for emission control and resource recovery: recent progress and challenges, Environ. Sci. Nano 9 (1) (2022) 81–104, https://doi.org/10.1039/D1EN00929J.

[2] T.N. Tu, T.M. Pham, Q.H. Nguyen, N.T. Tran, V.N. Le, L.H. Ngo, K. Chang, J. Kim, Metal–organic frameworks for aromatic-based VOC capture, Sep. Purif. Technol. 333 (2024) 125883, https://doi.org/10.1016/j.seppur.2023.125883.

[3] F. Yang, W. Li, R. Ou, Y. Lu, X. Dong, W. Tu, W. Zhu, X. Wang, L. Li, A. Yuan, J. Pan, Superb VOCs capture engineering carbon adsorbent derived from shaddock peel owning uncompromising thermal-stability and adsorption property, Chin. J. Chem. Eng. 47 (2022) 120–133, https://doi.org/10.1016/j.cjche.2021.02.013.

[4] R. Ou, W. Zhu, L. Li, X. Wang, Q. Wang, Q. Gao, A. Yuan, J. Pan, F. Yang, Boosted capture of volatile organic compounds in adsorption capacity and selectivity by rationally exploiting defect-engineering of UiO-66(Zr), Sep. Purif. Technol. 266 (2021) 118087, https://doi.org/10.1016/j.seppur.2020.118087.

[5] S. Zhang, L. Yao, B. Xu, L. Yang, Z. Dai, W. Jiang, Recent advances in zeolite-based materials for volatile organic compounds adsorption, Sep. Purif. Technol. 350 (2024) 127742, https://doi.org/10.1016/j.seppur.2024.127742.

[6] F. Yang, L.-A. Xing, X. Zhong, Y. Liu, Z. Guo, J. Yang, A. Yuan, J. Pan, Volatile acetic acid selective adsorption by biomass-derived activated carbon with humidity-resistance: tunable implanting and activation approach of activator, Sep. Purif. Technol. 341 (2024) 126891, https://doi.org/10.1016/j.seppur.2024.126891.

[7] E.J. Park, H.O. Seo, Y.D. Kim, Influence of humidity on the removal of volatile organic compounds using solid surfaces, Catal. Today 295 (2017) 3–13, https://doi.org/10.1016/j.cattod.2017.02.036.

[8] Y. Zhu, S. Guo, W. Liang, A literature review investigating the impact of temperature and humidity on volatile organic compound emissions from building materials, Build. Environ. 262 (2024) 111845, https://doi.org/10.1016/j.buildenv.2024.111845.

[9] X. Guo, X. Li, G. Gan, L. Wang, S. Fan, P. Wang, M.O. Tadé, S. Liu, Functionalized activated carbon for competing adsorption of volatile organic compounds and water, ACS Appl. Mater. Interfaces 13 (47) (2021) 56510–56518, https://doi.org/10.1021/acsami.1c18507.

[10] E. Hunter-Sellars, J.J. Tee, I.P. Parkin, D.R. Williams, Adsorption of volatile organic compounds by industrial porous materials: Impact of relative humidity, Microporous Mesoporous Mater. 298 (2020) 110090, https://doi.org/10.1016/j.micromeso.2020.110090.

[11] J.D. Holbrey, K.R. Seddon, Ionic liquids, Clean Prod. Process. 1 (4) (1999) 223–236, https://doi.org/10.1007/s100980050036.

[12] G. Cui, S. Lyu, F. Zhang, H. Wang, Z. Li, Y. Li, J. Wang, Tuning ionic liquids with functional anions for SO_2 capture through simultaneous cooperation of N and O chemical active sites with SO_2, Ind. Eng. Chem. Res. 59 (49) (2020) 21522–21529, https://doi.org/10.1021/acs.iecr.0c05190.

[13] T. Zhao, X. Yang, Z. Tu, X. Hu, Efficient SO_2 capture and conversion to cyclic sulfites by protic ionic liquid-based deep eutectic solvents under mild conditions, Sep. Purif. Technol. 318 (2023) 123981, https://doi.org/10.1016/j.seppur.2023.123981.

[14] L. Jiang, K. Mei, K. Chen, R. Dao, H. Li, C. Wang, Design and prediction for highly efficient SO_2 capture from flue gas by imidazolium ionic liquids, Green Energy Environ. 7 (1) (2022) 130–136, https://doi.org/10.1016/j.gee.2020.08.008.

[15] G. Cui, J. Zheng, X. Luo, W. Lin, F. Ding, H. Li, C. Wang, Tuning anion-functionalized ionic liquids for improved SO_2 capture, Angew. Chem., Int. Ed. 52 (40) (2013) 10620–10624, https://doi.org/10.1002/anie.201305234.

[16] R. Zhang, Q. Ke, Z. Zhang, B. Zhou, G. Cui, H. Lu, Tuning functionalized ionic liquids for CO_2 capture, Int. J. Mol. Sci. 23 (19) (2022) 11401, https://doi.org/10.3390/ijms231911401.

[17] X. Suo, Y. Fu, C.-L. Do-Thanh, L.-Q. Qiu, D.-E. Jiang, S.M. Mahurin, Z. Yang, S. Dai, CO_2 chemisorption behavior in conjugated carbanion-derived ionic liquids via carboxylic acid formation, J. Am. Chem. Soc. 144 (47) (2022) 21658–21663, https://doi.org/10.1021/jacs.2c09189.

[18] Y. Huang, G. Cui, Y. Zhao, H. Wang, Z. Li, S. Dai, J. Wang, Preorganization and cooperation for highly efficient and reversible capture of low-concentration CO_2 by ionic liquids, Angew. Chem., Int. Ed. 56 (43) (2017) 13293–13297, https://doi.org/10.1002/anie.201706280.

[19] F. Ding, X. He, X. Luo, W. Lin, K. Chen, H. Li, C. Wang, Highly efficient CO_2 capture by carbonyl-containing ionic liquids through Lewis acid-base and cooperative C-HO hydrogen bonding interaction strengthened by the anion, Chem. Commun. 50 (95) (2014) 15041–15044, https://doi.org/10.1039/c4cc06944g.

[20] R. Zhai, X. He, K. Mei, K. Chen, N. Cao, W. Lin, H. Li, C. Wang, Ultrahigh Nitric oxide capture by Tetrakis(azolyl)borate ionic liquid through multiple-sites uniform interaction, ACS Sustainable Chem. Eng. 9 (8) (2021) 3357–3362, https://doi.org/10.1021/acssuschemeng.1c00024.

[21] K. Chen, G. Shi, X. Zhou, H. Li, C. Wang, Highly efficient nitric oxide capture by azole-based ionic liquids through multiple-site absorption, Angew. Chem., Int. Ed. 55 (46) (2016) 14364–14368, https://doi.org/10.1002/anie.201607528.

[22] Y. Sun, S. Ren, Y. Hou, K. Zhang, Q. Zhang, W. Wu, Highly reversible and efficient absorption of low-concentration NO by amino-acid-based ionic liquids, ACS Sustainable Chem. Eng. 8 (8) (2020) 3283–3290, https://doi.org/10.1021/acssuschemeng.9b06923.

[23] J. Liu, Y. Xu, NOx absorption and conversion by ionic liquids, J. Hazard. Mater. 409 (2021) 124503, https://doi.org/10.1016/j.jhazmat.2020.124503.

[24] K. Li, K. Zong, X. Wang, G. Cui, D. Deng, Ionic liquids and deep eutectic solvents for NH_3 absorption and separation: a review, New J. Chem. 47 (46) (2023) 21426–21445, https://doi.org/10.1039/D3NJ04455F.

[25] R. Qiu, X. Luo, L. Yang, J. Li, X. Chen, C. Peng, J. Lin, Regulated threshold pressure of reversibly sigmoidal NH_3 absorption isotherm with ionic liquids, ACS Sustainable Chem. Eng. 8 (3) (2020) 1637–1643, https://doi.org/10.1021/acssuschemeng.9b06555.

[26] L. Peng, M. Shi, Y. Pan, Z. Tu, X. Hu, X. Zhang, Y. Wu, Ultrahigh carbon monoxide capture by novel protic cuprous-functionalized dicationic ionic liquids through complexation interactions, Chem. Eng. J. 451 (2023) 138519, https://doi.org/10.1016/j.cej.2022.138519.

[27] D.-J. Tao, F.-F. Chen, Z.-Q. Tian, K. Huang, S.M. Mahurin, D.-e. Jiang, S. Dai, Highly efficient carbon monoxide capture by carbanion-functionalized ionic liquids

through C-site interactions, Angew. Chem., Int. Ed. 56 (24) (2017) 6843–6847, https://doi.org/10.1002/anie.201701919.
[28] G. Cui, K. Jiang, H. Liu, Y. Zhou, Z. Zhang, R. Zhang, H. Lu, Highly efficient CO removal by active cuprous-based ternary deep eutectic solvents [HDEEA][Cl] + CuCl + EG, Sep. Purif. Technol. 274 (2021) 118985, https://doi.org/10.1016/j.seppur.2021.118985.
[29] Z. Zhou, P. Zhang, Y. Chang, X. Chen, Highly efficient capture and removal of H2S by multi-amine functionalized ionic liquids, J. Mol. Liq. 392 (2023) 123501, https://doi.org/10.1016/j.molliq.2023.123501.
[30] K. Huang, D.-N. Cai, Y.-L. Chen, Y.-T. Wu, X.-B. Hu, Z.-B. Zhang, Thermodynamic validation of 1-alkyl-3-methylimidazolium carboxylates as task-specific ionic liquids for H2S absorption, AIChE J. 59 (6) (2013) 2227–2235, https://doi.org/10.1002/aic.13976.
[31] M.J. Salar-García, V.M. Ortiz-Martínez, F.J. Hernández-Fernández, A.P. de los Ríos, J. Quesada-Medina, Ionic liquid technology to recover volatile organic compounds (VOCs), J. Hazard. Mater. 321 (2017) 484–499, https://doi.org/10.1016/j.jhazmat.2016.09.040.
[32] G. Li, K. Chen, Z. Lei, Z. Wei, Condensable gases capture with ionic liquids, Chem. Rev. 123 (16) (2023) 10258–10301, https://doi.org/10.1021/acs.chemrev.3c00175.
[33] S. Indra, R. Subramanian, S. Daschakraborty, Interaction of volatile organic compounds acetone and toluene with room temperature ionic liquid at the bulk and the liquid-vacuum interface, J. Mol. Liq. 331 (2021) 115608, https://doi.org/10.1016/j.molliq.2021.115608.
[34] R. Zhu, S. Huang, C. Gui, G. Li, Z. Lei, Capturing low-carbon alcohols from CO_2 gas with ionic liquids, Chem. Eng. Sci. 258 (2022) 117745, https://doi.org/10.1016/j.ces.2022.117745.
[35] M. Song, C. Gui, Z. Lei, Experimental and simulation studies on the capture of chlorinated volatile organic compounds by ionic liquids, Ind. Eng. Chem. Res. 62 (26) (2023) 10184–10194, https://doi.org/10.1021/acs.iecr.3c01163.
[36] Z. Wu, S. Shi, G. Zhan, F. Chang, Y. Bai, X. Zhang, J.C.S. Wu, S. Zeng, Ionic liquid screening for dichloromethane absorption by multi-scale simulations, Sep. Purif. Technol. 275 (2021) 119187, https://doi.org/10.1016/j.seppur.2021.119187.
[37] M. Mu, G. Yu, X. Zhang, R. Xu, N. Wang, B. Chen, C. Dai, Deep removal of dichloromethane using ionic liquids: thermodynamic and molecular insights, Chem. Eng. Sci. 284 (2024) 119498, https://doi.org/10.1016/j.ces.2023.119498.
[38] M. Mu, X. Zhang, G. Yu, C. Sun, R. Xu, N. Liu, N. Wang, B. Chen, C. Dai, Deep removal of chlorobenzene based volatile organic compounds from exhaust gas with ionic liquids, Sep. Purif. Technol. 298 (2022) 121610, https://doi.org/10.1016/j.seppur.2022.121610.
[39] W. Zhang, G. Li, Z. Chen, Z. Shang, P. Xu, Efficient capture of benzene and its homologues volatile organic compounds with protic [MIM][NTF2] and aprotic [EMIM][NTF2] ionic liquids: experimental and computational thermodynamics, J. Environ. Chem. Eng. 11 (5) (2023) 111124, https://doi.org/10.1016/j.jece.2023.111124.
[40] G. Yu, C. Dai, H. Gao, R. Zhu, X. Du, Z. Lei, Capturing condensable gases with ionic liquids, Ind. Eng. Chem. Res. 57 (36) (2018) 12202–12214, https://doi.org/10.1021/acs.iecr.8b02420.
[41] X. Ma, M. Wu, S. Liu, J. Huang, B. Sun, Y. Zhou, Q. Zhu, H. Lu, Concentration control of volatile organic compounds by ionic liquid absorption and desorption, Chin. J. Chem. Eng. 27 (10) (2019) 2383–2389, https://doi.org/10.1016/j.cjche.2018.12.019.
[42] X. Ma, W. Wang, C. Sun, J. Sun, Comprehensive evaluation of ionic liquid [Bmim][PF6] for absorbing toluene and acetone, Environ. Pollut. 285 (2021) 117675, https://doi.org/10.1016/j.envpol.2021.117675.
[43] W. Wang, X. Ma, S. Grimes, H. Cai, M. Zhang, Study on the absorbability, regeneration characteristics and thermal stability of ionic liquids for VOCs removal, Chem. Eng. J. 328 (2017) 353–359, https://doi.org/10.1016/j.cej.2017.06.178.
[44] V.C. Ramos, W. Han, K.L. Yeung, A comparative study between ionic liquid coating and counterparts in bulk for toluene absorption, Green Chem. Eng. 1 (2) (2020) 147–154, https://doi.org/10.1016/j.gce.2020.10.008.
[45] Z. Li, C. Dai, J. Zhu, Z. Lei, J. Zhang, G. Yu, Thermodynamics and molecular insights into anionic structural effects on toluene absorption with ionic liquids, Chem. Eng. Sci. 276 (2023) 118817, https://doi.org/10.1016/j.ces.2023.118817.
[46] I. Cichowska-Kopczyńska, M. Joskowska, B. Debski, R. Aranowski, J. Hupka, Separation of toluene from gas phase using supported imidazolium ionic liquid membrane, J. Membr. Sci. 566 (2018) 367–373, https://doi.org/10.1016/j.memsci.2018.08.058.
[47] W. Zhang, J. Yan, T. Sun, B. Zhang, X. Lan, C. Li, COSMO-SAC molecular screening method to analyze imidazole ionic liquids for toluene vapor absorption, CIESC J. 69 (5) (2018) 1829–1839, https://doi.org/10.11949/j.issn.0438-1157.20171228.
[48] J. Bedia, E. Ruiz, J. de Riva, V.R. Ferro, J. Palomar, J.J. Rodriguez, Optimized ionic liquids for toluene absorption, AIChE J. 59 (5) (2013) 1648–1656, https://doi.org/10.1002/aic.13926.
[49] A.-S. Rodriguez Castillo, P.-F. Biard, S. Guihéneuf, L. Paquin, A. Amrane, A. Couvert, Assessment of VOC absorption in hydrophobic ionic liquids: measurement of partition and diffusion coefficients and simulation of a packed column, Chem. Eng. J. 360 (2019) 1416–1426, https://doi.org/10.1016/j.cej.2018.10.146.
[50] G. Yu, M. Mu, J. Li, B. Wu, R. Xu, N. Liu, B. Chen, C. Dai, Imidazolium-based ionic liquids introduced into π-electron donors: highly efficient toluene capture, ACS Sustainable Chem. Eng. 8 (24) (2020) 9058–9069, https://doi.org/10.1021/acssuschemeng.0c02273.
[51] C. Zhang, J. Wu, R. Wang, E. Ma, L. Wu, J. Bai, J. Wang, Study of the toluene absorption capacity and mechanism of ionic liquids using COSMO-RS prediction and experimental verification, Green Energy Environ. 6 (3) (2021) 339–349, https://doi.org/10.1016/j.gee.2020.08.001.
[52] D. Warmińska, I. Cichowska-Kopczyńska, Thermodynamic study of binary mixtures of toluene with ionic liquids, 1-butyl-1-methylpyrrolidinium bis(trifluoromethylsulfonyl)imide, 1-hexyl-1-methylpyrrolidinium bis(trifluoromethylsulfonyl)imide and 1-butylpyridinium bis(trifluoromethylsulfonyl)imide, J. Mol. Liq. 304 (2020) 112754, https://doi.org/10.1016/j.molliq.2020.112754.
[53] T.U. Rashid, Ionic liquids: Innovative fluids for sustainable gas separation from industrial waste stream, J. Mol. Liq. 321 (2021) 114916, https://doi.org/10.1016/j.molliq.2020.114916.
[54] M. Zhu, P. Hu, Z. Tong, Z. Zhao, Z. Zhao, Enhanced hydrophobic MIL(Cr) metal-organic framework with high capacity and selectivity for benzene VOCs capture from high humid air, Chem. Eng. J. 313 (2017) 1122–1131, https://doi.org/10.1016/j.cej.2016.11.008.
[55] A.A. Rico-Barragán, J.R. Álvarez, S. Pioquinto-García, J. Rodríguez-Hernández, P. Rivas-García, N.E. Dávila-Guzmán, Cleaner production of metal-organic framework MIL-101(Cr) for toluene adsorption, Sustainable Prod. Consumption 40 (2023) 159–168, https://doi.org/10.1016/j.spc.2023.06.011.
[56] S. Zhang, Q. Yang, Z. Li, W. Wang, C. Wang, Z. Wang, Covalent organic frameworks as a novel fiber coating for solid-phase microextraction of volatile benzene homologues, Anal. Bioanal. Chem. 409 (13) (2017) 3429–3439, https://doi.org/10.1007/s00216-017-0286-x.
[57] H. Yuan, N. Li, J. Linghu, J. Dong, Y. Wang, A. Karmakar, J. Yuan, M. Li, P.J. S. Buenconsejo, G. Liu, H. Cai, S.J. Pennycook, N. Singh, D. Zhao, Chip-level integration of covalent organic frameworks for trace benzene sensing, ACS Sens. 5 (5) (2020) 1474–1481, https://doi.org/10.1021/acssensors.0c00495.
[58] L. Lan, Y. Huang, Z. Du, Y. Dan, L. Jiang, Visible light controllable adsorption-desorption of gaseous toluene on β-ketoenamine-linked porous organic polymer, Polymer 273 (2023) 125867, https://doi.org/10.1016/j.polymer.2023.125867.
[59] L. Tan, B. Tan, Hypercrosslinked porous polymer materials: design, synthesis, and applications, Chem. Soc. Rev. 46 (11) (2017) 3322–3356, https://doi.org/10.1039/C6CS00851H.
[60] L. Zhang, H. Yang, H. Zhang, Hyper-crosslinked dicationic ionic liquid porous polymers for nitrophenol adsorption, Microporous Mesoporous Mater. 342 (2022) 112118, https://doi.org/10.1016/j.micromeso.2022.112118.
[61] X. Suo, Y. Huang, Z. Li, H. Pan, X. Cui, H. Xing, Construction of anion-functionalized hypercrosslinked ionic porous polymers for efficient separation of bioactive molecules, Sci. China Mater. 65 (4) (2022) 1068–1075, https://doi.org/10.1007/s40843-021-1845-3.
[62] J. Gu, P. Shao, L. Luo, Y. Wang, T. Zhao, C. Yang, P. Chen, F. Liu, Microporous triazine-based ionic hyper-crosslinked polymers for efficient and selective separation of $H_2S/CH_4/N_2$, Sep. Purif. Technol. 285 (2022) 120377, https://doi.org/10.1016/j.seppur.2021.120377.
[63] M. Xu, J. Wang, L. Zhang, Q. Wang, W. Liu, Y. An, L. Hao, C. Wang, Z. Wang, Q. Wu, Construction of hydrophilic hypercrosslinked polymer based on natural kaempferol for highly effective extraction of 5-nitroimidazoles in environmental water, honey and fish samples, J. Hazard. Mater. 429 (2022) 128288, https://doi.org/10.1016/j.jhazmat.2022.128288.
[64] S. Raza, S. Nazeer, A. Abid, A. Kanwal, Recent research progress in the synthesis, characterization and applications of hyper cross-linked polymer, J. Polym. Res. 30 (11) (2023) 415, https://doi.org/10.1007/s10965-023-03783-7.
[65] R. Zhang, G. Cui, X. Wang, Y. Chen, X. Qiu, Q. Ke, D. Deng, C. Ge, H. Lu, S. Dai, Ionic liquid-based advanced porous organic hyper-crosslinked polymers (ILHCPs) for CO_2 capture and conversion, Chem. Eng. J. 489 (2024) 151102, https://doi.org/10.1016/j.cej.2024.151102.
[66] W. Li, W. Tu, J. Cheng, F. Yang, X. Wang, L. Li, D. Shang, X. Zhou, C. Yu, A. Yuan, J. Pan, Tuning N-doping thermal-process enables biomass-carbon surface modification for potential separation effect of $CO_2/CH_4/N_2$, Sep. Purif. Technol. 282 (2022) 120001, https://doi.org/10.1016/j.seppur.2021.120001.
[67] A.M. Najafi, S. Soltanali, H. Ghassabzadeh, Enhancing the CO_2, CH_4, and N_2 adsorption and kinetic performance on FAU zeolites for CO_2 capture from flue gas by metal incorporation technique, Chem. Eng. J. 468 (2023) 143719, https://doi.org/10.1016/j.cej.2023.143719.
[68] Q. Ke, Y. Xiong, M. Lu, G. Fang, G. Cui, P. Pan, F. Xiong, T. Wu, K. Huang, J. Min, C. Jin, H. Lu, Enhanced toluene adsorption over carbon–silica composite with promoted microporosity and moisture resistance, Sep. Purif. Technol. 344 (2024) 127268, https://doi.org/10.1016/j.seppur.2024.127268.
[69] S. Wen, T. Wang, X. Zhang, W. Xu, X. Hu, Y. Wu, Novel amino acid ionic liquids prepared via one-step lactam hydrolysis for the highly efficient capture of CO_2, AIChE J. 69 (11) (2023) e18206, https://doi.org/10.1002/aic.18206.
[70] M. Thommes, K. Kaneko, A.V. Neimark, J.P. Olivier, F. Rodriguez-Reinoso, J. Rouquerol, K.S.W. Sing, Physisorption of gases, with special reference to the evaluation of surface area and pore size distribution (IUPAC Technical Report), 87 (9-10) (2015) 1051-1069. https://doi.org/10.1515/pac-2014-1117.
[71] Y. Sang, J. Huang, Benzimidazole-based hyper-cross-linked poly(ionic liquid)s for efficient CO_2 capture and conversion, Chem. Eng. J. 385 (2020) 123973, https://doi.org/10.1016/j.cej.2019.123973.
[72] J. Gu, Y. Yuan, T. Zhao, F. Liu, Y. Xu, D.-J. Tao, Ionic-containing hyper-crosslinked polymer: a promising bifunctional material for CO_2 capture and conversion, Sep. Purif. Technol. 301 (2022) 121971, https://doi.org/10.1016/j.seppur.2022.121971.
[73] M. Li, L. Shi, Y. Liu, S. Li, W. Cui, W. Li, Y. Zhi, S. Shan, Y. Miao, A dual-ionic hyper-crosslinked polymer for efficient CO_2 fixation and conversion, Chem. Eng. J. 481 (2024) 148550, https://doi.org/10.1016/j.cej.2024.148550.

[74] W. Lyu, W. Zhang, H. Liu, Y. Liu, H. Zuo, C. Yan, C.F.J. Faul, A. Thomas, M. Zhu, Y. Liao, Conjugated microporous polymer network grafted carbon nanotube fibers with tunable redox activity for efficient flexible wearable energy storage, Chem. Mater. 32 (19) (2020) 8276–8285, https://doi.org/10.1021/acs.chemmater.0c02089.

[75] M. Herstedt, M. Smirnov, P. Johansson, M. Chami, J. Grondin, L. Servant, J. C. Lassègues, Spectroscopic characterization of the conformational states of the bis (trifluoromethanesulfonyl)imide anion (TFSI−), J. Raman Spectrosc. 36 (8) (2005) 762–770, https://doi.org/10.1002/jrs.1347.

[76] C. Liu, L. Shi, J. Zhang, J. Sun, One-pot synthesis of pyridine-based ionic hyper-cross-linked polymers with hierarchical pores for efficient CO_2 capture and catalytic conversion, Chem. Eng. J. 427 (2022) 131633, https://doi.org/10.1016/j.cej.2021.131633.

[77] X. Luan, S.J. Shah, X. Yu, R. Wang, J. Bao, L. Liu, J. Deng, Z. Zhao, Z. Zhao, Dual positive charging sites for MIL-101 enhanced adsorption of toluene under high humidity conditions: experimental and theoretical studies, Chem. Eng. J. 479 (2024) 147675, https://doi.org/10.1016/j.cej.2023.147675.

[78] M.J. Frisch, G.W. Trucks, H.B. Schlegel, G.E. Scuseria, M.A. Robb, J.R. Cheeseman, G. Scalmani, V. Barone, G.A. Petersson, H. Nakatsuji, X. Li, M. Caricato, A.V. Marenich, J. Bloino, B.G. Janesko, R. Gomperts, B. Mennucci, H.P. Hratchian, J.V. Ortiz, A.F. Izmaylov, J.L. Sonnenberg, D. Williams-Young, F. Ding, F. Lipparini, F. Egidi, J. Goings, B. Peng, A. Petrone, T. Henderson, D. Ranasinghe, V.G. Zakrzewski, J. Gao, N. Rega, G. Zheng, W. Liang, M. Hada, M. Ehara, K. Toyota, R. Fukuda, J. Hasegawa, M. Ishida, T. Nakajima, Y. Honda, O. Kitao, H. Nakai, T. Vreven, K. Throssell, J. Montgomery, J. A., J.E. Peralta, F. Ogliaro, M.J. Bearpark, J.J. Heyd, E.N. Brothers, K.N. Kudin, V.N. Staroverov, T.A. Keith, R. Kobayashi, J. Normand, K. Raghavachari, A.P. Rendell, J.C. Burant, S.S. Iyengar, J. Tomasi, M. Cossi, J.M. Millam, M. Klene, C. Adamo, R. Cammi, J.W. Ochterski, R.L. Martin, K. Morokuma, O. Farkas, J.B. Foresman, D.J. Fox, Gaussian 16 (Revision C.01), Gaussian, Inc., Wallingford CT, 2016.

[79] A.D. Becke, Density-functional thermochemistry. III. The role of exact exchange, J. Chem. Phys. 98 (7) (1993) 5648–5652, https://doi.org/10.1063/1.464913.

[80] C. Lee, W. Yang, R.G. Parr, Development of the Colle-Salvetti correlation-energy formula into a functional of the electron density, PhysRevB 37 (2) (1988) 785–789, https://doi.org/10.1103/PhysRevB.37.785.

[81] P.J. Stephens, F.J. Devlin, C.F. Chabalowski, M.J. Frisch, Ab initio calculation of vibrational absorption and circular dichroism spectra using density functional force fields, J. Phys. Chem. 98 (45) (1994) 11623–11627, https://doi.org/10.1021/j100096a001.

[82] A.D. Becke, Density-functional exchange-energy approximation with correct asymptotic behavior, PhysRevA 38 (6) (1988) 3098–3100, https://doi.org/10.1103/PhysRevA.38.3098.

[83] A. Bondi, van der Waals volumes and radii, J. Phys. Chem. 68 (3) (1964) 441–451, https://doi.org/10.1021/j100785a001.

[84] P. Liu, K. Cai, K. Wang, T. Zhao, D.-J. Tao, Highly defective HKUST-1 with excellent stability and SO_2 uptake: The hydrophobic armor effect of functionalized ionic liquids, Green Energy Environ. 9 (11) (2024) 1711–1723, https://doi.org/10.1016/j.gee.2023.10.003.